Studies on Stress-Strain Relationships of Polymeric Materials Used in Space Applications

NASA Award Number NCC 3-752
ORSSP Proposal Number: R5104

Final Report To

NASA Glenn Research Center
21000 Brookpark Road
Cleveland, OH 44136

Principal Investigator:
Dr. Sadhan C. Jana
Department of Polymer Engineering
University of Akron
Akron, OH 44325-0301

Co-investigator:
Dr. Alan Freed
Polymers Branch
NASA Glenn Research Center
21000 Brookpark Road
Cleveland, OH 44136

Post Doctoral Fellow:
Dr. David P. Gerrard
Department of Polymer Engineering
The University of Akron
Akron, Ohio 44325-0301

April 8, 2002

Summary

A two-year research plan was undertaken in association with Polymers Branch, NASA Glenn Research Center, to carry out experimental and modeling work relating stress and strain behavior of polymeric materials, especially elastomers and vulcanized rubber.

An experimental system based on MTS A/T-4 test facility environment has been developed for a broader range of polymeric materials in addition to a design of laser compatible temperature control chamber for online measurements of various strains. Necessary material processing has been accomplished including rubber compounding and thermoplastic elastomer processing via injection molding.

A broad suite of testing methodologies has been identified to reveal the complex non-linear mechanical behaviors of rubbery materials when subjected to complex modes of deformation. This suite of tests required the conceptualization, design and development of new specimen geometries, test fixtures, and test systems including development of a new laser based technique to measure large multi-axial deformations. Test data has been generated for some of these new fixtures and has revealed some complex coupling effects generated during multi-axial deformations.

In addition, fundamental research has been conducted concerning the foundation principles of rubber thermodynamics and resulting theories of rubber elasticity. Studies have been completed on morphological properties of several thermoplastic elastomers. Finally, a series of steps have been identified to further advance the goals of NASA's ongoing effort.

I. Introduction

A long-term effort to properly characterize the material mechanical properties of vulcanized rubber and other elastomers has recently started and is ongoing at NASA's Glenn Research Center. This effort has been substantially advanced by the recent work conducted by University of Akron Researchers. Over the 2001 fiscal year, a diverse set of goals has been met.

Modifications to the MTS A/T-4 test facility environment to allow for a broader range of material testing have been made. Necessary material processing has been accomplished including rubber compounding and thermoplastic elastomer processing via injection molding. A broad suite of testing methodologies has been identified that promises to reveal the complex non-linear mechanical behaviors of rubbery materials when subjected to complex modes of deformation.

This suite of tests required the conceptualization, design and development of new specimen geometries, test fixtures, and test systems including development of a new laser based technique to measure large multi-axial deformations. Test data has been generated for some of these new fixtures and has revealed some complex coupling effects generated during multi-axial deformations.

Fundamental research has been conducted concerning the foundation principles of rubber thermodynamics and resulting theories of rubber elasticity. Studies have been completed on morphological properties of several thermoplastic elastomers. Finally, a series of steps have been identified to further advance the goals of NASA's ongoing effort.

II. Facility Modifications

The facility environment for the elastomer mechanical testing has been modified to accommodate the newly developed suite of testing. These modifications (centered around the MTS 858 A/T-4 Machine, located in Room 107, Building 49 at NASA Glenn) include:

1) Design, fabrication, and installation of an enclosure that enables low and high temperature (-100 to +100 °C) testing of rubber specimens using laser micrometers or other optical techniques to measure specimen deformations and rotations;
2) Installation of a dedicated supply of nitrogen gas to the MTS A/T-4's new environmental enclosure;
3) Installation of a dedicated electrical circuit to the A/T-4 and supporting electronics to enable R/F noise isolation and suppression if required and which provides the required current and power capacity for additional electronic devices.
4) Design and fabrication of a dedicated electronics cabinet to house all of the required supporting hardware and to allow for easy access via breakout panel to all of the MTS Test Star Controller inputs and outputs. Items housed in the electronics cabinet include a) a 4-axis digital servo-electric motor controller; b) 3 servo electric motor amplifiers; c) 3 laser micrometer controllers; d) 4 strain gage/load cell signal amplifier/controllers with digital readouts.
5) Design and fabrication of several mounting devices which provide the required flexibility/utility to enable the positioning of the multiple accessories needed for a diverse suite of tests.

III. Material Processing

Current and potential future work relating to the efforts underway at NASA concerning elastomer mechanical properties required the processing of both thermoplastic elastomers and industrially important rubber compounds. The full line of general purpose SANTOPRENE® thermoplastic elastomer, (Grades 101-55, 101-64, 101-73, 101-80, 101-87, 103-40, and 103-50), was processed using two techniques.

Utilizing an injection molding process, ASTM standard tensile, Izod impact, and Charpy impact specimens were produced. Using an extrusion process cylindrical rod and pipe specimens were produced of varying cross-section and diameter, which in part depended on the process ability of each SANTOPRENE® Grade.

Eleven vulcanized rubber recipes were compounded. These include: an unfilled natural rubber; three filled natural rubbers (25,50 and 75 pph carbon black); a filled styrene butadiene rubber (FSBR), (50 pph carbon black); a filled butyl rubber (FBR), (50 pph CB); a filled NBR (50 pph CB); three filled neoprenes (25,50 and 75 pph CB); and a filled EPDM (100 pph CB). These formulations are representative of materials used in industry. Specific recipes for each are given in Figure 1. At least 2 kilograms of each compound were produced. Mooney rheometer cure curves were supplied with each compound.

IV. Experimental Mechanics of Materials

Although the constitutive behavior of rubber-like materials has been widely studied and discussed for many years, a great deal of work still needs to be done on the subject, especially with regards to potentially non-linear coupling interactions between multi-axial modes of deformation. Existing constitutive models, based on empiricism or on "The physics of long chain networks", require multi-axial experimental data to define the constitutive model constants if they are to properly predict multi-axial behavior.

More than just stress/strain data generated in uni-axial tension testing is required to properly define a rubber material's behavior under different modes of deformation. Although constitutive model constants can be fitted with pure uni-axial tension data, the models will not predict with the same accuracy the material's simple shear or equal-biaxial extension responses. Likewise even if uni-axial tension, equal-biaxial tension and simple shear data are used to fit a model's constants, all models will not always predict other multi-axial responses.

The dissertation work of Kadlowec [1] provides a clear example of the failure of standard tests to generate the required sensitivity in constitutive constants to adequately predict even the most slightly complex multi-axial deformations. Kadlowec experimentally measured the effect of static torsion on the

radial stiffness response of rubber bushings. She measured an initial softening of the radial stiffness at low levels of torsion followed by an increase in radial stiffness at higher levels of torsional strain.

She created a finite element model of the bushing deformation, using material constants generated with data from a uni-axial extension, equal bi-axial extension and simple shear test data. She generated the predicted response using several models including the Ogden, 3rd order polynomial and the Arruda-Boyce models. Despite the fact that the constitutive constants used for each analysis were generated by a relatively complete set of data, the formulation of Ogden was the only one capable of predicting qualitatively the bushing's softening and then hardening behavior that was measured experimentally. However, the Ogden model was unable to quantitatively predict the response of the bushing.

Kadlowec's work, like many others', highlights the need for the development of simple experimental techniques designed to isolate and reveal quantitatively the potential coupling generated by multi-axial states of deformation. Such a requirement has led to the identification of a suite of experiments with the specimen geometries, loading conditions, and measurements required to more fully define constitutive equation constants. Groups of data generated from this suite will form the basis for the development of refinements to existing constitutive models. Eventually these data sets may drive conceptualization of entirely new material models based on the newly revealed physics of long chain rubbery networks.

Three basic specimen geometries have been identified for the suite of tests: a) flat sheet, b) solid cylinder, and c) cylindrical bushing. The required deformation modes for these geometries are listed below. They are depicted schematically in Figure 2.

1)Simple shear of a flat sheet
2)Simple tension of a solid cylinder
3)Simple compression of a solid cylinder
4)Pure shear of a flat sheet
5)Volumetric compression of a solid cylinder
6)Torsional shear of a solid cylinder
7)Simple shear with static compression/dilation of a flat sheet
8)Simple tension and torsional shear of a solid cylinder
9)Proportional/non-proportional planar extension of a flat sheet
10)Volumetric compression with static torsional shear of a solid cylinder
11)Proportional/non-proportional bi-axial shear of a cylindrical bushing
12)Proportional/non-proportional bi-axial shear with added radial tension/compression of a cylindrical bushing

The first four tests listed above are industry and academic standards routinely used to quantify a rubber's response to simple/uniaxial deformations. They must be performed in order to evaluate the more complex deformations.

A solid cylinder shaped specimen geometry was chosen over the planar sheet geometry for the simple tension and compression experiments because it allows for more accurate measurements of Poisson's ratio and can be more easily adapted to multi-axial modes of deformation.

Assumptions of rubber incompressibility although necessary for the development of the simplest analytical formulation, must be challenged if one attempts to ascertain second order/coupling effects. Measuring simple bulk response and the effects of pre-imposed states of deviatoric strain on bulk response is extremely important to the full development of constitutive laws that incorporate potential coupling between different modes of deformation. Therefore, Tests 5 and 10 are intended to reveal the material's Bulk response and potential coupling interactions between dilational and deviatoric deformations.

The ability to perform the majority of the suite of tests listed above required the conceptualization, design and fabrication of several new fixtures to hold the various specimens and generate the required modes of deformation. For the test types that involve multi-axial loading conditions, the existing axial/torsional capability of the MTS 858 test rig was found adequate in most cases. However, in some cases, additional actuation systems were/are required. These will be discussed in more detail below.

An advanced dual lap shear test fixture capable of performing test types 1 and 7 has been designed and fabricated at the University of Akron. It is depicted in Figure 3. Using the rotary actuation capabilities of the MTS 858, it generates controlled deformation in the sample sheet's thickness direction. A left and right handed ball screw/ pressure plate design converts the rotation of the MTS cross head to outward lateral movement of each of the inner plates molded to the two specimen sheets. Axial movement of the cross head generates prescribed levels of shear by moving the specimens' inner plates relative to their outer plates which are themselves each fixed to an outer supporting plate.

The forces generated in the direction of specimen thickness are measured with four load cells. Each load cell is connected to opposite corners of the outer supporting plates via coupling nuts and ball joint rod ends. Each outer supporting plate is mounted to a laterally moving connecting block via a linear bearing/rod pivoting connection. The connecting blocks are mounted to the main lower support block on linear shafting/linear bearings, which allow un-impeded motion of the connecting blocks and outer supporting plates in the lateral direction. Thus, the unimpeded motion of the outer supporting plates in the lateral direction and the pivoting nature of the corner connections together isolate the normal loads into the instrumented linkages.

Test types 2,3, 6, and 8 required design of the new laser based axial-torsional- diametral test measurement system described below. It also required the design of a mounting fixture that was capable of holding a rubber specimen subject to large axial and torsional loads and corresponding large strains of over a wide range of temperatures.

Some of the specimens to be tested were to be processed via extrusion. The ability of standard adhesives such as CHEMLOCK to maintaining rigid contact between surfaces at elevated temperatures is often uncertain. Based on these issues, a set of re-usable mechanical grips were designed and fabricated to hold the specimen.

The steel gripping fixtures consist of two cylindrical portions of different outer diameters. The cylindrical sample slides down into a circular cavity in the largest diameter portion until touching the ledge inside the fixture that separates the two portions of the fixture. Two rows of four threaded holes in this top portion allow for the application of set screws/steel plungers into the specimen to prevent the specimen from rotating during a test.

The smaller diameter portion of the fixture has a threaded inner diameter for adding extensions. The outer diameter of the lower portion is 25 mm to fit into existing machine mounting clamps. A wood screw is inserted through the hole in the sample ledge and turned tight into the centerline of the sample. The threads on the screw share the axial load generated on the sample with the set screws/plungers of the larger diameter portion.

Measurements of the diameter of specimens mounted in these fixtures were made when the sample was tested to large extensions and rotations. The edge effects generated by these fixtures were defined by the axial length of specimen exhibiting a non-constant diameter under a fixed level of strain. These edge effects were confined to a zone of material within three set screw diameters from the location of the set screw prior to loading (on the order of 18 mm from the set screw location). In comparison, for a specimen of the same diameter that was bonded to a flat substrate, the region of material experiencing edge effects was on the order of three sample diameters, (in this case on the order of 55 mm.)

The specimen geometries needed to accomplish Test Types 4 and 9 (pure shear of a sheet and proportional/non-proportional planar extension of a flat sheet) are depicted in Figure 4 along with the fixtures required to hold the specimens. These specimen geometries are commonly used in academia and can be fabricated very easily in simple compression molds.

Test 9 requires the design and fabrication of a stand alone fixture, conceptualized in Figure 5. Two sets of servo actuators, amplifiers, screw jacks, load cells, and load cell amplifier/ readout /controller have been identified and purchased for use on this fixture when built.

A new fixture assembly designed to accomplish the requirements of tests 5 and 10 (volumetric compression of a solid cylinder and volumetric compression with static torsional shear of a solid cylinder) has been conceptualized, designed and built, schematically shown in Figure 6. It consists of four stainless steel pieces of circular cross-section.

The top and bottom pieces are machined to 25 mm outer diameter for mounting into existing clamps. The bottom portion of the top piece has been machined to an outer diameter of 0.75 inch and is 2 inches long. The cylinder piece of the assembly is a long cylinder with inner diameter bored out to .751" and is 1.75" long. The aligning base piece of the assembly has a .75" diameter section .5" long and a 1" long section of 25mm diameter. The 25mm diameter face has a .25" wide, .125" deep slot machined across it for a .25" square key. The bottom piece is a 25mm diameter solid cylinder with a .25" wide .125" deep slot machined across it. The slot/keyway in the bottom two pieces of the assembly is required because of the current slight cross head misalignment of the A/T-4 MTS 858.

A specimen is bonded to the top and aligning pieces. Then the assembly is placed in the MTS machine with a .25" key through the slot in the lower interface allowing fine tuning alignment of the entire fixture/specimen assembly in one direction. A torsional strain can then be applied to the cylindrical specimen. Once the torsional pre-strain is set, the cylinder piece is slid over the twisted specimen. As the cross-head and top piece move down in the axial direction, the specimen is put into a state of volumetric compression imposed on a pre-existing state of torsional shear. The change in volume can be calculated base on the axial displacement and the change in inner diameter of the cylinder piece. This change can be assumed to be negligible or can be calculated by measuring the change in outer diameter with strain gages or with optical devices such as the laser micrometer described below.

The fixture capable of generating axial, torsional, and radial deformations of bushing shaped specimens as required by tests 11 and 12 has been conceptualized, designed, and fabricated. The new 3-D bushing test fixture is shown in Figure 7. The fixture consists of a bottom flange, which mounts to a bottom mounting plate. This interface aids in fixture/crosshead alignment. Two side plates are mounted to the bottom mounting plate and are connected to each other via 8 horizontal pairs of 3/4" linear shafting. Along each of the top two pairs and bottom two pairs of shafting slides a center shaft support block. Each block contains three linear bearings, two for the horizontal shafting and a third oriented vertically between the two horizontal bearings. The horizontal travel of each center shafting support blocks can fixed using a set of single piece shaft collars.

Along the middle two pairs of shafting slide a specimen clamping assembly. This clamping assembly consists of two pieces. One piece contains four horizontal linear bearings and a mounting hole on the outboard side for connection to the radial actuation device described below. The second piece of the clamp assembly contains four oversized holes through which the linear shafting pass and four counter board holes for socket head cap screws. Each piece has opposite halves of a through hole machine out between their contacting faces. When connected to one another, the clamp assembly generates a circular cavity with an outer diameter that matches the outer diameter of the bushing specimens.

An upper shaft with a threaded hole at its bottom end is mounted to the actuator of the MTS cross head. It slides vertically through the bearings in the upper two center support blocks and is connected to the threaded end of the lower shaft. The lower shaft slides vertically in the bottom two center shafting support blocks. The upper portion of the lower shaft has a threaded end and a section machined down to fit the inner diameter of the bushing specimen. It extends through the inner steel sleeve of the bushing specimen when mounted in the clamp assembly.

When tightened, the upper shaft/inner sleeve/lower shaft assembly provides the capability to generate axial and torsional strains in the bushing specimen by generating relative displacements and rotations between the inner sleeve of the bushing and its clamped outer sleeve. The upper shaft/inner sleeve/lower shaft assembly along with the four center shafting support blocks and shaft collars provide the resistance required to conduct radial loading of the bushing concurrently with axial and torsional loading.

When radial loading of the bushing is desired a radial actuation system is added to the fixture. Components for the radial actuation system have been collected. They include an electric servo motor and shaft coupling which drive a 2-ton machine screw jack. The screw jack is mounted to a side plate of the main fixture by four bars. The moving screw of the jack is centered between the four bars and has a flange end to which is mounted a tension/compression load cell. A rod threaded into the center of the load cell passes through a hole in the Side Plate and is threaded into a hole in the sliding portion of the specimen clamp assembly.

The load cell measures the radial load on the bushing and can be used as part of a control feed back loop to generate prescribed levels of radial load on the bushing generated by relative radial movements of the specimen clamp assembly and the specimen inner sleeve. The servomotor encoder signal can be used as control feedback for the generation of prescribed levels of relative radial displacement.

V. Laser Based Deformation Measurements

Rubber goods usually possess the ability to maintain their shape without fracture after withstanding large levels of tension, compression, and shear strain. This unique capability, while securing rubber's niche as an engineering material, creates serious problems for experimentalist interested in quantifying, analyzing, and predicting its behavior during finite complex deformations. The main stumbling block encountered has been the lack of instrumentation capable of withstanding the high levels of deformation that are easily managed by the rubber.

Strain gages can be used to measure rubber's strain response to a complex stress field, as long as the deformation is restricted to the region defined as small stain, i.e. less than ~30%. For strain regimes falling in the moderate to large range, optical methods have been developed. One of the most common of these involve using laser extensometers during uniaxial tension, compression or proportional bi-axial tension tests. During the test the extensometer unit emits a band of laser light at the specimen. The strategic placement of special reflective tape defines a specimen's gage section. The laser light reflected back from the tape is received back at the extensometer unit. On board electronics filter the return signal and provide the user the relative position of the reflective tape thereby enabling measurements of gage strain.

The accuracy of the extensometer method is limited by several factors. The process of using reflected laser light limits the inherent accuracy of extensometer systems. The resolution of such a system decreases with increasing beam length and is advertised as to be on the order of microns.

More importantly, application of rigid adhesive tape to the deforming rubber surface generates a source of random error. Depending on which portion of the rubber contact surface maintains adhesion with the tape, the tape can tilt in either direction or remain aligned during a test. Often, the researcher must attempt to compensate for this random error by substantially increasing the number of samples tested.

Another popular optical method involves using a camera and zoom lens connected to a computer equipped with the required hardware and software to digitize "captured" images of the deforming sample. The sample is marked with objects strategically fixed to the specimen's surface and chosen to provide the greatest optical contrast with the surface of the specimen. Although this method is able to monitor local complex deformation fields, its accuracy and utility are limited by many factors including image pixel size versus field of view tradeoffs, sample curvatures, massive size of each sample data set, and relatively slow sampling rates ~30 per second.

Studies of the simple deformation behavior of rubber are now commonplace using the systems described above. However, if one wants to measure the full state of strain produced in rubber when subject

to non-simple deformations such as the non-proportional torsional shear/uni-axial tension of rubber cylinders, these methods can be replaced by another optically based technique which addresses some of the other systems' deficiencies.

A detailed description of this new technique is offered below. The abilities of the new technique to expose stress/strain de-coupling effects during stress relaxation and to explore common Poisson's Ratio/Incompressibility Assumptions are highlighted.

Laser micrometers are commonly used as processing aids for wire and cable extrusion processes. They serve as the feedback portion of closed loop control circuits designed to maintain tight control of an extrudate's cross-section. Unlike laser extensometers, the laser micrometers consist of three units rather than just one. A laser beam is transmitted at the object or objects of interest by the transmitter unit. The portions of the laser beam not obstructed by the objects are received by the receiver unit. The third unit, the controller, processes the received signal and records the positions of all of the shadow edges generated by the objects of interest.

The operator can specify analog outputs from the controller that are generated based on calculations using simple mathematical operations on any combination of the shadow edges' positions. The advertised resolutions of these instruments are on the order of .1-1 micron and boast sampling rates greater than 600 per second.

Three laser micrometers are used together with NASA Glenn's MTS 858 Axial Torsional Test Machine to form a system capable of ascertaining the entire state of strain produced in rubber cylinder specimens experiencing finite uni-axial tension/compression deformations concurrently with finite torsional shear rotations. This has been made possible by the development of special clips (A/T Laser Gage Clips) attached to the specimen, which define its gage section and in conjunction with the laser micrometers, permit measurements of the relative rotations and displacements at the gage boundaries.

Figure 8 offers a schematic view of the test system. One laser group (i.e. transmitter and receiver pair) measures the specimen's diameter. It is referred to here as the Diametral Laser, (Beta LaserMike Brand, Model 162). Its beam is oriented horizontally and its axial position is controlled using a servo motor/digital controller/linear slide sub-system. In addition to measuring changes in specimen diameter during a test, it can be used to measure the full distributions of diameters/sample width across a sample's length and as a function of angular position in order to ascertain processing irregularities, gripping effects and permanent set.

The other two laser groups (the upper and lower A/T lasers, Beta LaserMike Brand, Model 179) are rigidly mounted to columns of the MTS machine. Their laser beams pass vertically along the side of the specimen and monitor the shadows generated by the displacing and rotating A/T laser gage clips.

The required calculations involving specific shadow edge positions are programmed using the laser manufacturer's software and are downloaded as firmware to the controllers (Beta LaserMike Brand, Intellipacs). The calculated results are made available real time through the same software and are used to generate two analog outputs per laser controller.

Figure 9 is a schematic of a rod specimen, mechanical grips and A/T laser gage clips assembly. The A/T laser gage clips are designed to relay sample displacement and rotation information while accommodating large changes in the specimen diameter. They are simply stainless steel cylinders with precision machined and ground helical edge surfaces. Four threaded holes evenly spaced around the circumference at the clip mid-section provide the mounting for four steel plungers that attach the clip to the specimen at distinct register points.

The desired positions of the clips are registered on the sample prior to mounting on the MTS 858. Four register points are placed 90° apart along the sample circumference at two axial positions separated by the desired initial gage distance. Depending on the material and test profile, the registers can be generated non-intrusively using a simple ink pen or can be physical registers generated by using a small heated point or machined using a drill bit.

Each clip is slid over the sample to the proper axial and angular position. The steel plungers equipped with specially designed tips to match the register are released in controlled order to engage the register points, fixing each clip and defining the specimen's gage section.

Each laser micrometer is calibrated using two NIST traceable calibration pins the size of which are selected based on the size range of the objects to be measured. To increase the accuracy of the calibration, the pins are positioned within the beam at the expected location of the measured objects. A special fixture was designed and fabricated to enable calibration of the three laser systems concurrently.

The displacements and rotations of the A/T laser gage clips are calibrated using the LVDT and rotary potentiometer of the MTS machine. With the lower end of the sample free to move, prescribed displacements and rotations of the clips are generated using the MTS controller and the corresponding displacement and rotation signals fed back from the Laser A/T controllers are scaled accordingly.

VI. Preliminary Test Results

There have been two main goals for this course of research. One has been the definition of a suite of experiments required for proper constitutive model development. The other was the development of the physical tools required to carry out the experimental suite so defined. Although the generation of full data sets was not a feasible goal, some preliminary experiments were conducted with several of the new tools. These are described below.

Volumetric Compression of a Solid SANTOPRENE® Cylinder

The bulk response of SANTOPRENE® Grade 101-73 Thermoplastic elastomer was measured using the fixture described above. Several interesting observations resulted from these experiments. The SANTOPRENE®, which is a mixture of EPDM and polypropylene, exhibited two distinct zones of bulk behavior. As the downward movement of the cross head forced the specimen into a dilatational mode of deformation, a relatively soft initial bulk response abruptly changed into one that was rapidly stiffening. While the dilation was held fixed, the normal load, i.e. hydrostatic stress, relaxed by about 5% over 2 minutes of time. The material exhibited permanent set after removing the axial compression and recovered along both regions of stiffness, suggesting that the initially soft region is caused by the inherent structure of the SANTOPRENE®.

This behavior is characteristic of foam material and suggests that for this grade of SANTOPRENE®, rapid cooling of the extrudate during processing may have created micro-voids near the regions of Polypropylene. Figure 10 gives the time plots of the axial load and displacement. Figure 11 is a plot of load versus displacement (which is of identical form to a plot of pressure versus dilation).

Laser Based Measurements on Axial Torsion Deformations of Solid SANTOPRENE® Cylinders

An example of the capability of the laser based measurement system to measure specimen shape is given in Figure 12. Diameter is plotted against rotation angle for an extruded SANTOPRENE® rod specimen unclamped at its lower end. As shown from the figure, the particular specimen had a non-circular cross-section. This type of information, so easily revealed by the laser system, can be generated as a function of axial position and used to evaluate processing techniques, gripping effects and used to improve other critical analysis's. The particular specimen from the Figure could have been discarded or its non-circular cross-section corrected by annealing it in a rigid cylindrical container under pressure.

Some initial studies were performed with SANTOPRENE® Grade 101-73 extruded rod. The mechanical mounting fixtures described above were used to mount the specimens to the MTS. The samples were 18.8 mm in diameter with a clip gage section of 72.46 mm. The set of laser gage clips used for these tests possessed an outer circumference height that varied at the rate of 10.16 mm/360 degrees to a maximum of 20 mm. An example of the rotation calibration for these clips is given in Figure 13. As can

be seen from the Figure, the raw laser outputs vary linearly with prescribed rotations and therefore can be easily converted into relative rotations between the limits of the gage section, (i.e. torsional strain). The output for the axial calibration is similar to that for the torsional.

The specimens underwent simple deformation controlled loading profiles which consisted of three cycles each consisting of four steps. After a prescribed deformation at a constant deformation rate, the deformation was held for a prescribed length of time. The deformation was then reversed and a second hold step was done. In the first cycle the deformation mode was an axial pull. In the second cycle, the mode was a torsional twist. The third cycle involved a concurrent pull and twist to the same magnitudes generated in the first and second cycles. The loading profile established the material's uniaxial and shear responses, revealed the material's relaxation behavior and also exposed cross coupling between the two modes of deformation.

Figure 14 plots the raw displacement/load signal data for a sample undergoing the loading profile. Figure 15 plots the effect of torsional twist on the relative axial displacements between laser clips during the axial deformations with and without a concurrent twist. The concurrent twist generates a smaller relative axial displacement within the gage section and therefore a smaller gage strain for the same prescribed axial displacement at the crosshead grips.

Figure 16 plots the change in sample diameter measured for the axial pull cycle. Now a true stress/strain curve can be plotted for the gage section isolated by the laser clips, Figure 17. The concurrent twist effectively softens the axial response for this case with similar results measured over a fairly broad range of deformations.

The relaxation steps revealed interesting behaviors as well. Figure 18 plots the relaxing axial load following the isolated axial pull versus time along with relaxing axial gage strain. Figure 19 plots specimen diameter versus the relaxing axial load. The relaxation of load is accompanied by (or caused by) a redistribution of deformation across the specimen. Finally, the relaxing axial true stress is plotted in Figure 20 along with the dilation strain calculated for the gage section.

The modulation in specimen gage section dimensions during the load relaxation accounts for some but not all of the relaxation effect on the axial stress. It is possible that these effects are created by the technique used to hold the specimen. These tests should be repeated with specimens mounted to a rigid substrate via an adhesive to examine the potential influence of the mechanical grips.

Axial-Torsional Testing of Rubber Bushing Specimens

Bi-axial shear tests were performed with the help of Dr. Jennifer Kadlowec, a NASA Summer Faculty, using the 3-D bushing test fixture described above. The specimens, fabricated by Clevite Corp of Ohio, are depicted in Figure 21 and are identical to the ones described in reference [1]. They are made from a filled NR that was molded onto a steel inner sleeve. The outer steel sleeve was swage compressed and bonded over the rubber's outer diameter.

A series of tests were performed to ascertain the effects of concurrent axial and torsional loading on the bushing's axial and torsional stiffness'. The loading profiles for these tests consisted of 20 cycles of 4 steps. During the first step a prescribed axial displacement and torsional rotation was imposed on the specimen. This loading step was followed by a hold step to allow for relaxation. Then an unloading step was performed where the displacement and rotation imposed in the first step was removed. The final step was another hold step.

In order to determine the relative effect of one mode of deformation on the other mode, two basic types of profiles were performed. In the first type, the cyclic displacement maximum was set to a constant and the rotation maximum was incrementally increased during the first 10 cycles and then incrementally decreased during the last 10 cycles. In the second basic type of profile, the cyclic rotation maximum was set to a constant while the axial displacement maximum was increased and then decreased. The ramping up and then down of the second deformation mode gave two data points for each displacement/deformation pair per profile, and produced the ability to determine setting effects.

Before testing, each specimen was worked in by cycling it ten times to 110% of the maximum axial displacement and rotation in order to reduce the initial transients exhibited by filled rubber vulcanizates. Figure 22 is a plot of the load and torque output generated during a test in which the effect of changing displacement maximum effected the required torque for a rotation of 20 degrees.

Similar profiles were generated for a range of rotation angles (5, 10, 15, and 20 degrees) and axial displacements (2, 4, 6, 8, 10 mm). The level of strains generated by these displacements and rotations ranged from 24% to 120% axial strain and 10% to 40% torsional strain.

The effect of concurrent axial shear strain generated by axial displacement on the relative torsional response (relaxed, as measured at the end of the hold step) is given in Figure 23. The axial shear generates a softening and then hardening of the torsional stiffness as compared to the baseline generated with no concurrent axial displacement. The hardening point, defined as the axial displacement at which the

torsional response begins to harden for a given torsional rotation, gets smaller as the degree of torsional rotation increases.

The effect of torsional shear generated by rotational twist on the absolute axial load response is plotted in Figure 24. Here the torsional shear produces no clear effect on the axial shear response. The fact that the different modes of deformation were effected differently by each other raises puzzling questions.

These differences may be due to the fact that the two modes of shear deformation are different from each other. The axial shear is a more pure mode of deformation as compared to the torsional shear in the sense that as the angle of twist increases in torsional shear, the kinematics of the fixed boundaries produce added uniaxial components of strain to the strain field. In the case of the axial deformation imposed shear, the strain field is relatively unaffected by the kinematics of the deformation, however, there are substantial changes of the edge profile which may result in indeterminate effects at the edges. In torsional shear, the profile of the free ends of the rubber cylinder remain unchanged during the deformation.

The fact that the specimens were prepared with a substantial amount of swage induced radial pre-stress may add to the relative differences in effects on the two shear modes. The axial displacement may effectively unload this pre-stress while the torsional rotation may not.

The effect of the second mode of deformation on the relaxation response was also investigated in order to determine the basic nature of the multi-axial effects and the extent to which they are influenced by stress relaxation within the rubber/filler matrix. One series of tests involved imposing a prescribed torsion rotation and holding it, and then imposing a prescribed level of axial displacement at different times during the torsional relaxation. The axial deformation was removed and the resulting effect on the still relaxing torque was monitored.

The results of such a loading sequence is given in Figure 25. The addition of the second mode of shear reduces the torque required to hold the rotation, and when the axial shear is removed, some but not all of the torque is recovered suggesting that the added deformation has an elastic and viscous effect on the response from the primary mode. The magnitudes of the elastic and viscous effects appear to depend on the relative level of axial and torsional deformation, but not on the time at which the axial deformation is applied. The added axial shear appears to accelerate/augment the relaxation of the torsional stress.

VII. Rubber Thermodynamics and Elasticity

The development of new constitutive models describing rubber material mechanical behavior requires solution of fundamental thermodynamic relationships. The assumption that the heat capacity of rubber is

independent of strain is a foundation of the widely accepted statistical theory of rubber elasticity as described by Treloar [2] which attributes rubber elasticity mainly to entropy and the Second Law of Thermodynamics. However, over a half a century ago several different researchers examined the potential effects of strain on the heat capacity of rubber and reported conflicting results. The publicized discrepancy and its potential impact on established fundamental theories provided the justification for a re-examination of the potential effects of strain level on heat capacity.

Ornstein et al [3] measured a substantial dependence of an unfilled Natural Rubber's heat capacity on strain level. Later, Boissonnas [4] and then Mayor [5], using a completely different technique than Ornstein, measured no clear effect.

Ornstein stretched rubber band shaped specimens over copper plates of varying length that were bent along their width into the shape of cylinders. The copper cylinder and rubber sample were brought to elevated temperature (80°C) and allowed to come to equilibrium. After reaching equilibrium at the elevated temperature they were inserted into a calorimeter filled with water. The rise of the water temperature to equilibrium was measured using a mercury thermometer arrangement and was used to calculate the heat capacity of the rubber at different levels of stretch. A schematic of the sample is given in Figure 26.

The results of the experiments, reproduced in Figure 27, suggest a strong and substantial dependence of heat capacity with strain. As strain was increased from 0 to 100% the rubber's average specific heat over the range of ~ 22-80° C fell by nearly a third and then increased back to the un-stretched value at a strain of 200%. It should be pointed out here that Nah, et al [6] has recently measured the effect of temperature on the specific heat of rubber. In the range of 45 to 95°C, all rubber compounds tested exhibited specific heats which monotonically increased with temperature at total rates less than +10%/50°C.

Boissonnas [4] and Mayor [5] used a technique that was completely different than Ornstein [3] and reported completely different results. In the case of Boissonnas, rubber strips (1-2 mm thick) were cut from rubber sheets and stretched to given extensions with known weights. The strips were then wound over a cylindrical shaped electrical heating element which consisted of a .2 mm diameter constantan wire wound over a thin walled copper tube (10 mm diameter, 75 mm Long, and .1 mm thick). A thermocouple measured the specimen temperature, with one junction placed between the rubber strip and the wire and the other junction inserted into a hole at the center of a 70 gram copper block.

The assembly was placed in a glass container that was held under vacuum. The glass container was then inserted into a Dewar Flask for added insulation. The specific heat of the entire system was calculated based on the measured change in thermocouple temperature output after application of a known amount of

current/power through the heating element. The specific heat of the rubber was found by subtracting the heat capacity of the assembly without the rubber specimen from the total system heat capacity and then dividing by the mass of the rubber sample. A schematic of the test sample is given in Figure 28.

Mayor reproduced the experiments of Boissonnas with a slightly modified set up. Instead of using a copper tube for support he used a 15 mm diameter Dellite roll (made of Bakelite paper) with 3-4 mm thick rubber specimens and a platinum wire to measure temperature. His results and those of Boissonnas directly conflicted with those of Ornstein. In Boissonnas' experiments, increasing strain over the range reported by Ornstein produced a constant heat capacity for a vulcanized Natural Rubber and a relatively slight increase in heat capacity with increasing strain for an un-vulcanized natural rubber. In Mayor's experiments, increasing strain over the same range produced a constant heat capacity for a un-vulcanized Natural Rubber and a relatively slight increase in heat capacity with increasing strain for a vulcanized natural rubber.

It would seem that based on the published results of Boissonnas and Mayor, the assumption that heat capacity does not change with strain was accepted as a basis for the formulation of the widely accepted entropy based theory of rubber elasticity as described by Treloar [1]. However, a careful review of these results suggests that the issue be re-examined experimentally because several parts of the technique and results of Boissonnas and Mayor raise important questions.

The first question arises from the sparse set of data published by Boissonnas. For the vulcanized natural rubber, only three extensions are evaluated (0,65, and 195% strain). The second question relates to the geometry and mounting configuration of the rubber specimens. By bending the stretched specimens over the curvature of the supporting cylinders, the authors imposed a varying state of strain through the cross-section of the sample in the plane of specimen thickness. If one assumes linear elastic pure bending and rubber incompressibility, the difference in strain across the cross-section is greatest for 0% strain, ranging from -21% to +21% for the 4 mm thick specimen of Mayor. The importance of this issue is magnified even more by the limited set of data points generated.

A third question involves thermodynamics and the location of the thermocouple for these experiments. For these experiments, the thermocouple wire is placed between the stretched and wound rubber and the wound heating wire. The changing level of tension in the rubber would cause a changing level of pressure and real contact area across the rubber/thermocouple/ heating element contact and the rubber/heating element contact. Changes in specimen strain, i.e. the test's "independent" variable, therefore would generate additional variations in heat transfer rates, which themselves would modify the system thermodynamics. In other words, changes in the "independent" variable also effect processes that ideally should not vary with the independent variable.

Ornsteins' technique is devoid of the last concerns. Complex states of strain are isolated to small regions of the bands lying over the edges of the bent copper plates. The measurements of specimen temperature occur in a fixed medium, i.e. the water bath, were heat transfer rates to the Thermocouple are not affected by changes in specimen stretch. Ornstein's method is the simpler of the two and is therefore preferable from an experimental point of view.

Based on these observations a test program was begun to re-examine the potential effects of strain on the heat capacity of rubber. A simple calorimeter arrangement was assembled and two new fixtures designed and built which permit examination of the effects of both tension and compression strains on the heat capacity of rubber.

The fixtures are depicted in Figure 29. Identical band-shaped specimen geometries are used in both fixtures. Each fixture enables testing over a full range of strain requiring only one calibration of heat content per fixture.

The initial series of tests were conducted using a pair of Dewers (with I.D. of 2 and 3/4 inches by eleven inches tall) filled with known quantities of water. One bath was held at room temperature and the other filled with water brought to elevated temperature (>60°C). The temperature distribution in each water bath was measured using two OMEGA brand thermister thermocouples, one located at the top and the other at the bottom of each bath. The readout devices for each thermister were connected to a computer via serial ports enabling logging of the measured temperature at the rate of two readings per second. Although the data output from the thermister readout were given in °C to the third decimal, the accuracy and resolution of the thermisters were advertised to be 0.01 °C, a substantial improvement over standard thermocouples.

The strained rubber specimens and fixtures were inserted into the hot water bath and allowed to come to a state of thermal quasi-equilibrium. This point being defined as the moment that the temperature drop in the hot water flask reached a relatively constant rate. After this point, the sample/fixture were moved from the hot water bath and into the room temperature bath.

Quasi-equilibrium of the room temperature bath was defined as the point at which the heating of the bath stopped and the bath began cooling back to room temperature. Based on the average temperatures of the baths before and after moving the specimen and measuring the mass of water in the room temperature bath before and after specimen transfer, the heat capacity of the specimen fixture assembly could be calculated.

Unfortunately, this technique produced conflicting trends in large part due to the variation in corrections that had to be made based on the amount of hot water that was transferred with each specimen and the evaporative cooling that occurred during the transfer.

However, the utility of the thermister/computer logging devices and the fixtures that were built offer future workers a foundation to pursue this very important issue. Based on the lessons learned during the initial study, several recommendations can be offered which in large part follow more closely the experiments of Ornstein.

The specimen/fixture assembly should be brought to elevated temperature in an inert atmosphere if possible and maintained at the temperature for at least a half hour. Then the fixture should be moved into a Dewar type vessel filled with water held at room temperature. Thermisters should be used to measure the temperature gradient across the fluid height as the water bath heats up. Vertically moving the submerged fixture slowly with a steel wire will promote mixing as described by Ornstein. Again, definition of a quasi equilibrium point would be critical, occurring near the point at which the bath temperature begins to drop back to room temperature.

VIII: Conclusions and Suggestions for Future Work

The capability to conduct multi-axial testing of elastomers at NASA Glenn has been significantly augmented as a result of the work conducted by University of Akron personnel under during the 2001 Fiscal Year. Several necessary facility modifications have been made. A proper suite of experiments have been identified to reveal potential coupling inter actions between the various modes of deformation. In order to conduct the recommended suite of tests, several new test apparatus had to be conceptualized, designed, and fabricated. These new experimental tools include a laser based axial-torsional-diametral test measurement system, an axial/torsional/radial bushing test fixture, an advanced dual lap shear test fixture, a volumetric compression with static torsional shear test fixture.

Data generated with some of these new tools were also presented. These initial experiments have confirmed the belief that cross coupling between deformation modes in non-linear materials is a subject that has yet to be quantitatively or even qualitatively predicted by many of the constitutive models that are currently used to predict rubber behavior. The work should therefore systematically proceed, utilizing the new experimental tools that have been created. Finally, the research concerning the potential effects of strain on the heat capacity of rubber should be continued with the new techniques recommended in the previous section. The potential impact of finishing these basic thermodynamic experiments can not be overstated.

References

[1] Kadlowec, J. A., PhD Dissertation, University of Michigan (1999)

[2] Treloar, L.R.G., "The Physics of Rubber Elasticity", Clarendon Press, Oxford, 3rd Edition (1975).

[3] Ornstein, D. S., Woods, J., Eymers, J. G.; *Rubber Chem. Technol.*, **3**, 403 (1930)

[4] Boissonnas, C. G.; *Rubber Chem. Technol.*, **12**, 794 (1939)

[5] Mayor, A.; *Rubber Chem. Technol.*, **21**, 112 (1948)

[6] Nah, C. Park, J. H., Cho, C. T., Chang, Y., Kaang, S.; J. Applied Polymer Science, **72**, 1513 (1999)

List of Figures

Figure 14: Raw displacement/load signal data for a SANTOPRENE Grade 101-73 sample undergoing a loading profile consisting of a simple torsional twist, a simple axial pull, then a concurrent torsional twist and axial pull.

Figure 15: The effect of torsional twist on the relative axial displacements between laser clips during the axial deformations with and without a concurrent twist of a SANTOPRENE Grade 101-73 rod.

Figure 16: Change in sample diameter with axial gage strain measured during the simple axial pull of SANTOPRENE Grade 101-73 rod.

Figure 17: True Stress versus True Gage Strain curve plotted for the gage section of a SANTOPRENE Grade 101-73 rod, isolated by A/T laser clips. The concurrent twist effectively softens the axial response.

Figure 18: Relaxation of axial load and axial gage strain following isolated axial pull of a SANTOPRENE Grade 101-73 rod.

Figure 19: Relaxation of axial load and diameter change following isolated axial pull of a SANTOPRENE Grade 101-73 rod.

Figure 20: Relaxation of dilation and axial gage stress following isolated axial pull of a SANTOPRENE Grade 101-73 rod.

Figure 21: Bushing Test Specimen Geometry.

Figure 22: Load and torque output generated during a rubber bushing test in which the effect of changing displacement maximum effected the required torque for a rotation of 20 degrees.

Figure 23: The effect of concurrent axial shear strain generated by axial displacement on the relative torsional response of a rubber bushing. The axial shear generates a softening and then hardening of the torsional stiffness as compared to the baseline generated with no concurrent axial displacement.

Figure 24: The effect of torsional shear generated by rotational twist on the absolute axial load response of a rubber bushing. The torsional shear produces no clear effect on the axial shear response.

Figure 25: The effect of axial shear deformation on the relaxing torque required to hold fixed the rotational twist of a rubber bushing. The added deformation has an elastic and viscous effect on the response from the primary mode. The added axial shear appears to accelerate/augment the relaxation of the torsional stress.

Figure 26: A schematic of the specimen and mounting used by Ornstein et al [3]. Stretched rubber band shaped specimens were stretched over copper plates of varying length that were bent along their width into the shape of cylinders.

Figure 27: The results of Ornstein's experiments [3] suggest a strong and substantial dependence of heat capacity with strain. As strain was increased from 0 to 100% the rubber's average specific heat over the range of ~ 22-80° C fell by nearly a third and then increased back to the un-stretched value at a strain of 200%. The results of Boissonnas [4] are plotted as well.

Figure 28: The specimen/mounting geometry of Boissonnas [4], rubber strips (1-2 mm thick) were cut from rubber sheets and stretched to given extensions with known weights. The strips were then wound over a cylindrical shaped electrical heating element.

Figure 29: Schematic of test fixtures designed to examine effects of tension and compression strain on the heat capacity of rubber.

An Unfilled Natural Rubber Formulation

Ingredient	Amount (phr*)
Natural rubber	100
Process oil	2
Stearic acid	2
Zinc oxide	5
Antioxidant: 6PPD	1
Sulfur	2.75
Cure accelerator: benzothiazyl disulfide	1
Cure accelerator: tetramethyl thiuram disulfide	0.1

*Parts by weight per 100 parts by weight of rubber

Cure: 10 minutes at 150°C

Shore A Hardness 39
Tensile Strength (MPa) 24
Breaking Elongation (%) 750

An Ethylene-Propylene Diene Monomer (EPDM) Formulation

Ingredient	Amount (phr*)
EPDM (Nordel 2744)	100
Extender: paraffinic process oil	90
N-550 carbon black	100
Zinc oxide	5
Stearic acid	1
Sulfur	2
Cure accelerator: mercaptobenzothiazole	1.0
Cure accelerator: tetramethylthiuram monosulfide	1.5

*Parts by weight per 100 parts by weight of rubber

Cure: 20 minutes at 166°C

Shore A Hardness 64
300% Modulus (MPa) 6.8
Tensile Strength (MPa) 15.5
Breaking Elongation (%) 410

A Typical Styrene-Butadiene Rubber (SBR) Formulation

Ingredient	Amount (phr*)
SBR-1500	100
Process oil	4
Stearic acid	1
Zinc oxide	5
Antioxidant: DPPD	1.5
N-330 carbon black	50
Sulfur	2
Cure accelerator: benzothiazyl disulfide	2
Cure accelerator: tetramethyl thiuram disulfide	0.15

*Parts by weight per 100 parts by weight of rubber

Cure 25 minutes at 150°C

Shore A Hardness 65
300% Modulus (MPa) 13.5
Tensile Strength (MPa) 25
Breaking Elongation (%) 500

Carbon Black Filled Natural Rubber Formulations For General-Purpose Engineering Use

Ingredient	Amount (phr*)
Natural rubber	100
Process oil	5
Stearic acid	2
Zinc oxide	5
N-550 carbon black	25, 50, 75
Phenylamine antioxidant	1.5
Sulfur	2.5
Cure accelerator: benzothiazyl disulfide	1.0
Cure accelerator: tetramethyl thiuram disulfide	0.1

*Parts by weight per 100 parts by weight of rubber

Cure: 20 minutes at 150°C

	N550 carbon black (phr)		
	25	50	75
Shore A Hardness	51	62	72
300% Modulus (MPa)	7	9	11
Tensile Strength (MPa)	22	24	25
Breaking Elongation (%)	700	600	550

A Butyl Rubber Formulation

Ingredient	Amount (phr*)
Butyl 268	100
Process oil	2
Stearic acid	1
Zinc oxide	5
N-330 carbon black	50
Sulfur	2
Cure accelerator: tetramethyl thiuram disulfide	1
Cure accelerator: mercaptobenzothiazole	0.5

*Parts by weight per 100 parts by weight of rubber

Cure: 20 minutes at 171°C

Shore A Hardness 62
300% Modulus (MPa) 8.5
Tensile Strength (MPa) 16.3
Breaking Elongation (%) 530

An Acrylonitrile-Butadiene Rubber (NBR) Formulation

Ingredient	Amount (phr*)
NBR (Chemigum N689B)	100
Process aid	2
N330 carbon black	50
Zinc oxide	5
Stearic acid	1.5
Sulfur	1.75
Antioxidant: octylated diphenylamines	1.5
Plasticizer: dibutyl phthalate	12.5
Coumarone-indene resin	12.5
Cure accelerator: benzothiazyl disulfide	1.5

*Parts by weight per 100 parts by weight of rubber

Cure: 35 minutes at 150°C

Shore A Hardness 59
300% Modulus (MPa) 9.2
Tensile Strength (MPa) 18.5
Breaking Elongation (%) 510

Polychloroprene Formulations For General-Purpose Engineering Use

Ingredient	Amount (phr*)
Polychloroprene (Neuprene W)	100
Process aid	5
N550 carbon black	25, 50, 75
Stearic acid	2
Zinc oxide	5
Magnesium oxide	4
Antioxidant: octylated diphenylamine	2
Cure accelerator: activated thiadazine	1

*Parts by weight per 100 parts by weight of rubber

Cure: 20 minutes at 150°C

	N550 carbon black (phr)		
	25	50	75
Shore A Hardness	53	64	78
300% Modulus (MPa)	9	11	14
Tensile Strength (MPa)	20	21	24
Breaking Elongation (%)	400	350	300

Figure 1: Compound recipes and typical mechanical properties of eleven rubber compounds supplied for elastomer testing.

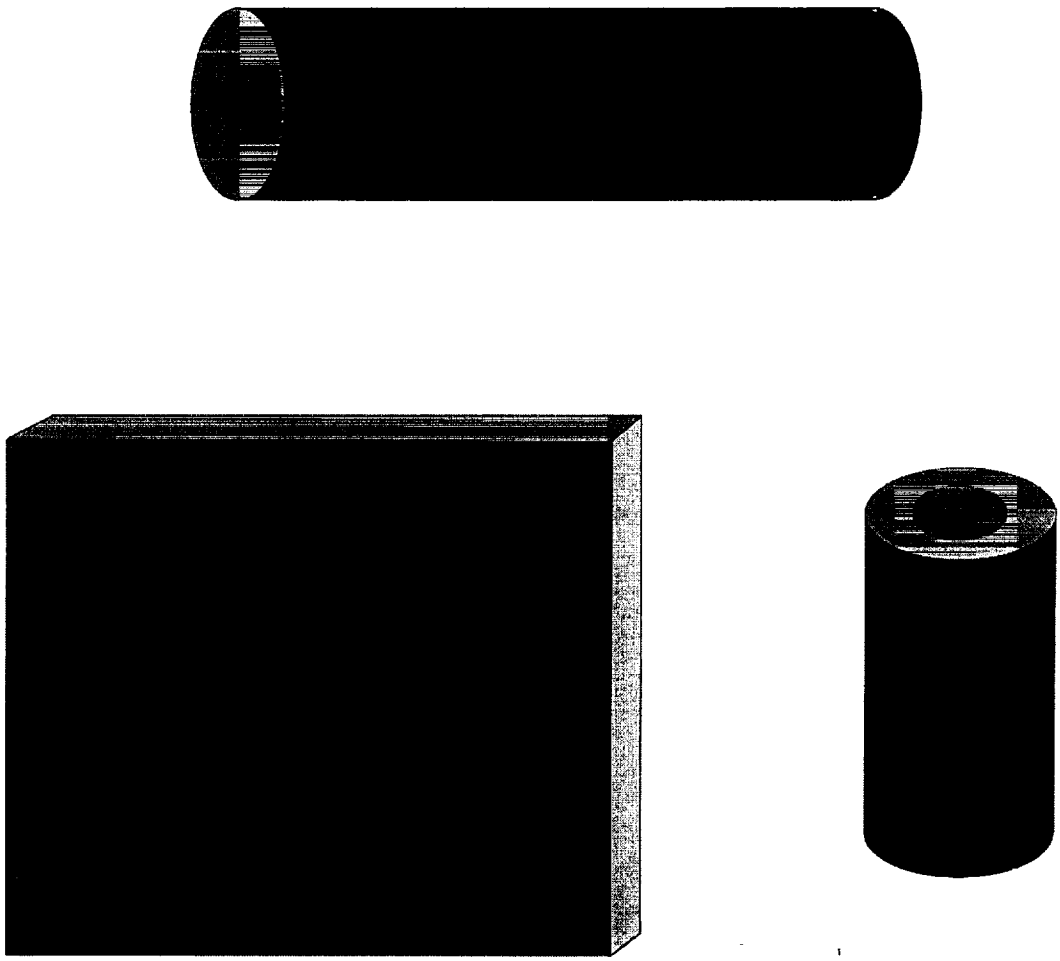

Figure 2: Three basic specimen geometries identified for the suite of multi-axial tests: flat sheet, solid cylinder, and cylindrical bushing.

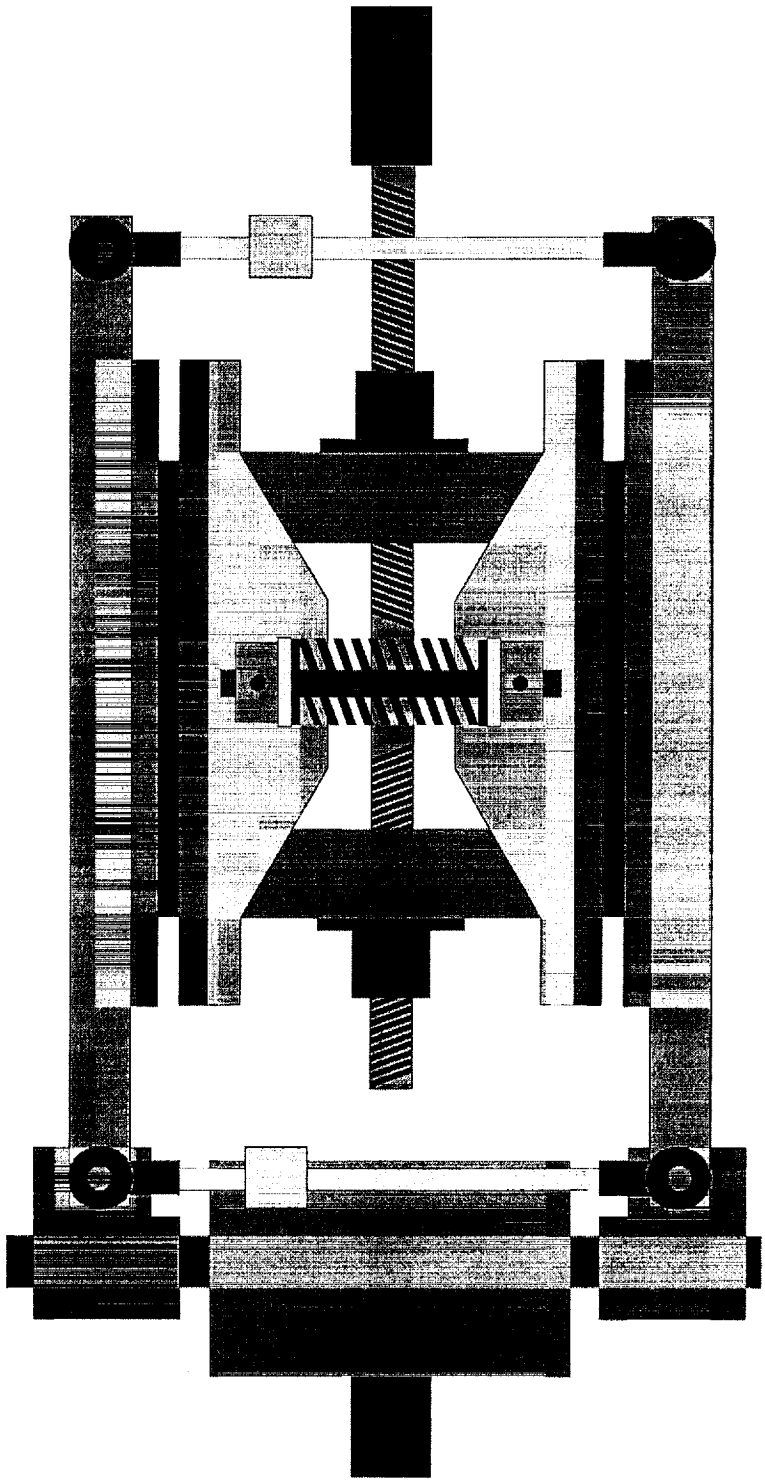

Figure 3: Advanced dual lap shear test fixture for testing simple shear of a flat sheet and simple shear with static compression/dilation of a flat sheet.

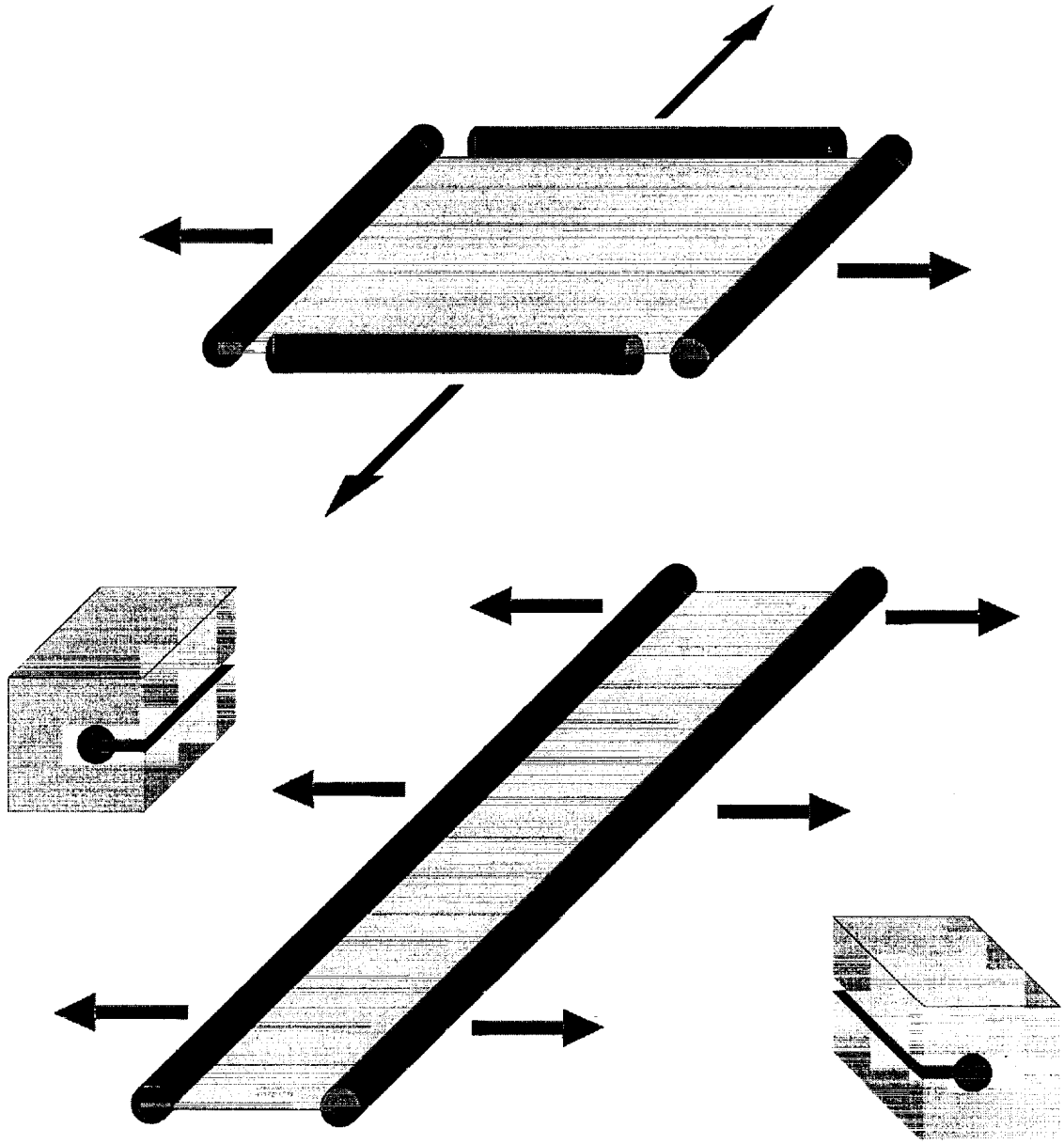

Figure 4: A schematic of the specimen geometries needed to accomplish pure shear of a sheet and proportional/non-proportional planar extension of a flat sheet along with the fixtures required to hold the specimens.

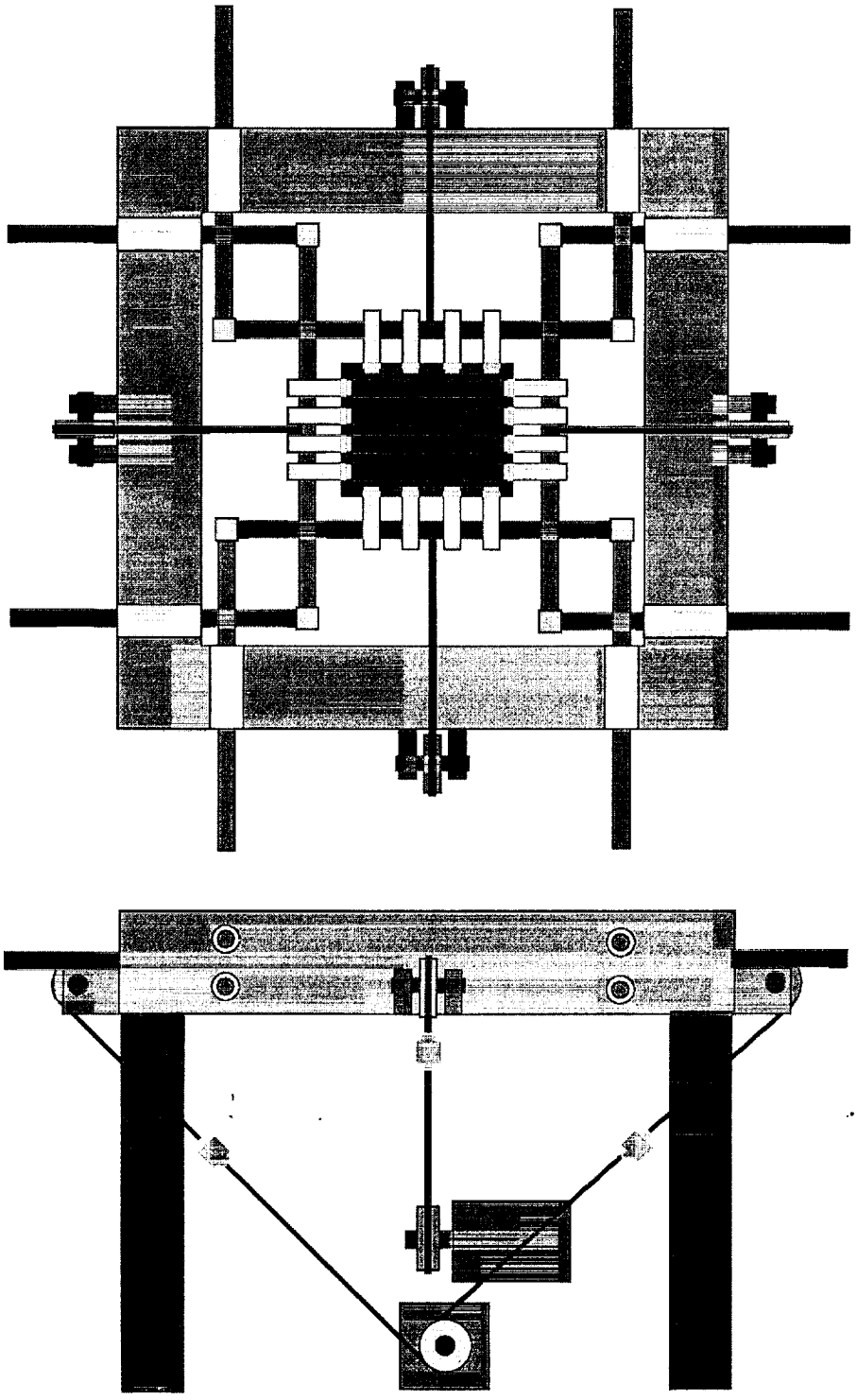

Figure 5: Schematic of an apparatus capable of accomplishing proportional/non-proportional planar extension of a flat sheet

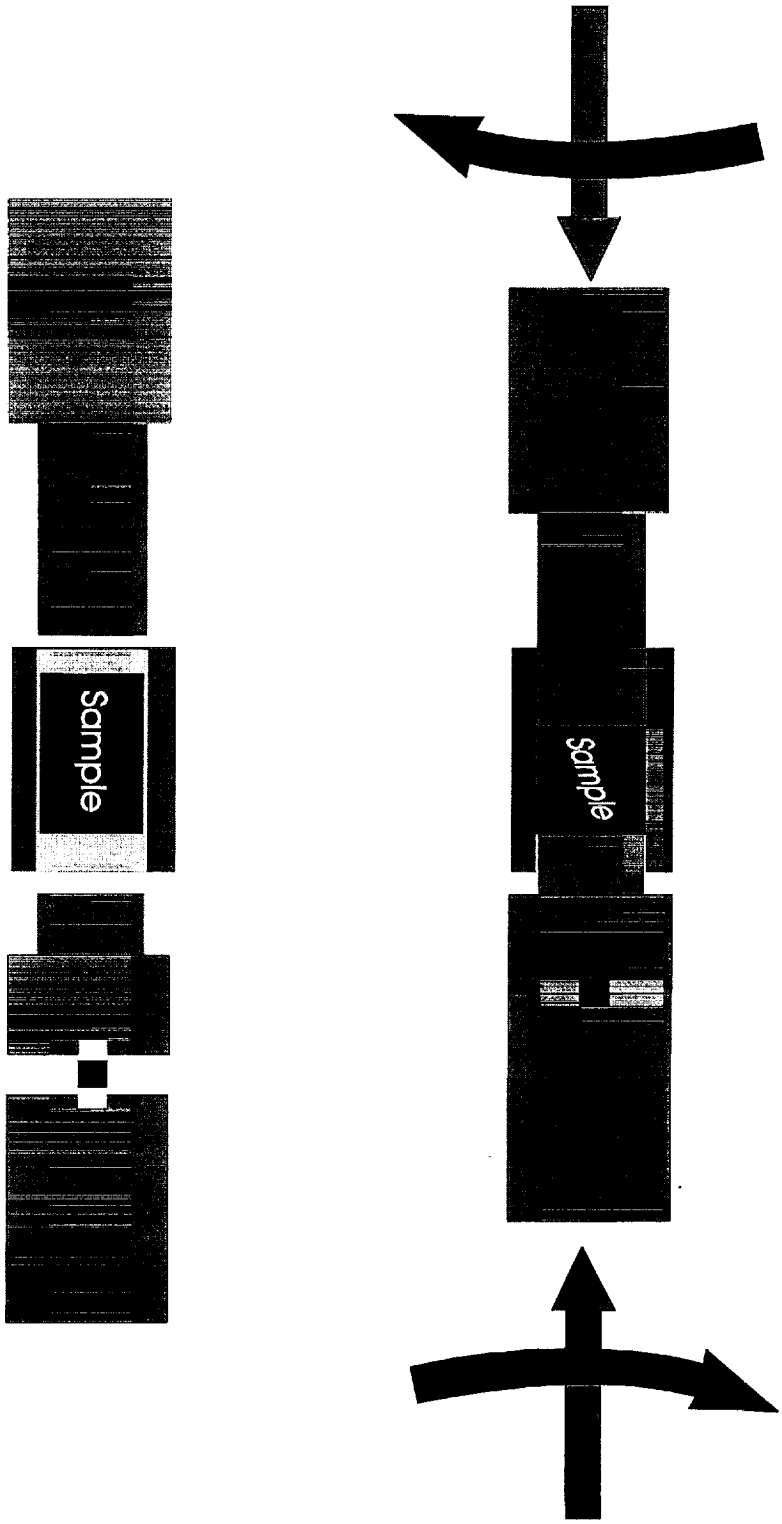

Figure 6: Schematic of the fixture that generates volumetric compression of a solid cylinder and volumetric compression with static torsional shear of a solid cylinder.

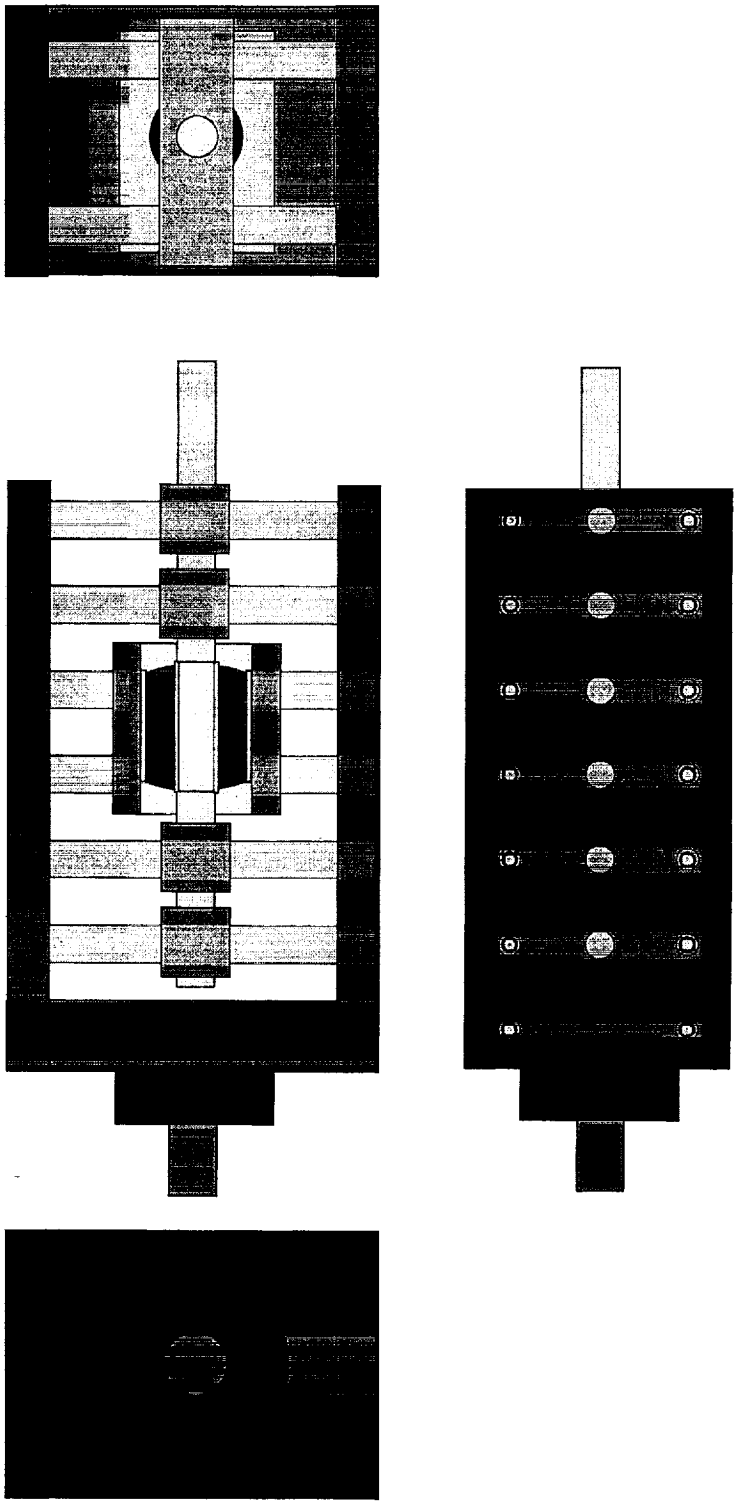

Figure 7: New 3-D bushing test fixture capable of generating axial, torsional and radial loading of bushing specimens.

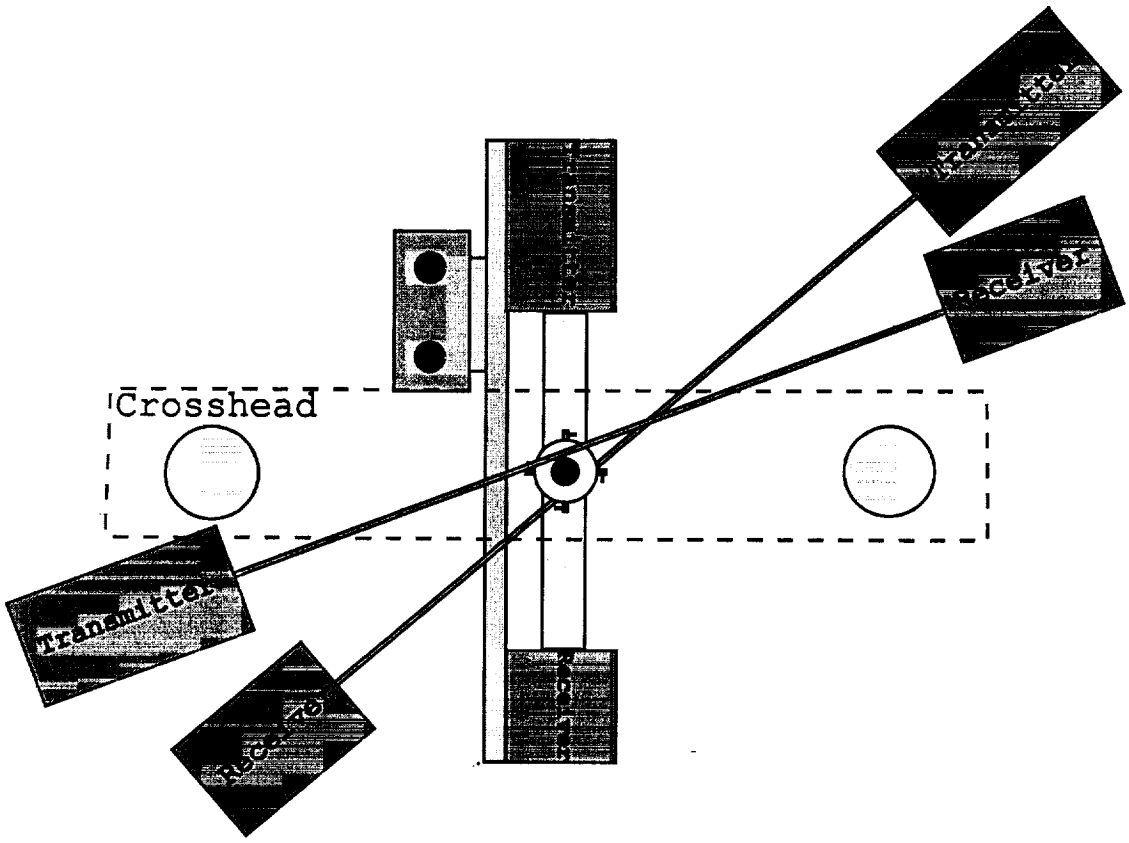

Figure 8: Top view schematic of the laser based axial/torsional/ diametral strain measurement system.

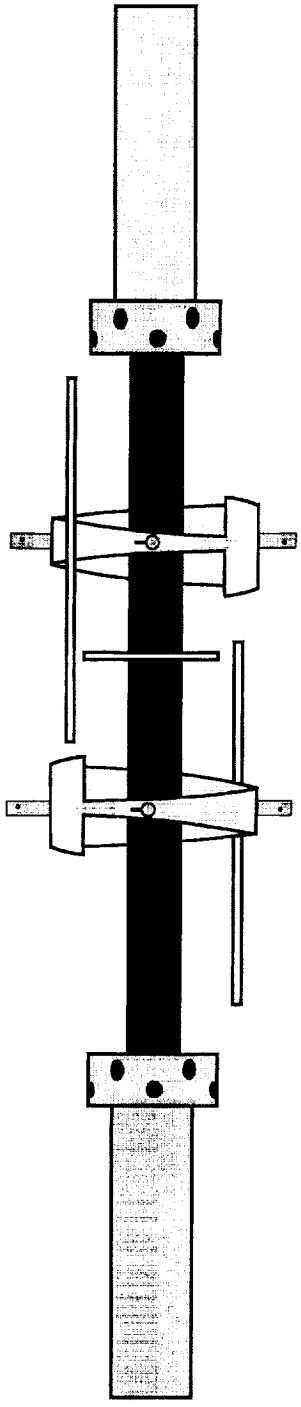

Figure 9: Schematic of a rod specimen, mechanical grips and A/T laser gage clips assembled with laser micrometer beam paths shown as two vertical lines (each crossing over a gage clip from a different direction) and one horizontal line crossing over the specimen gage diameter.

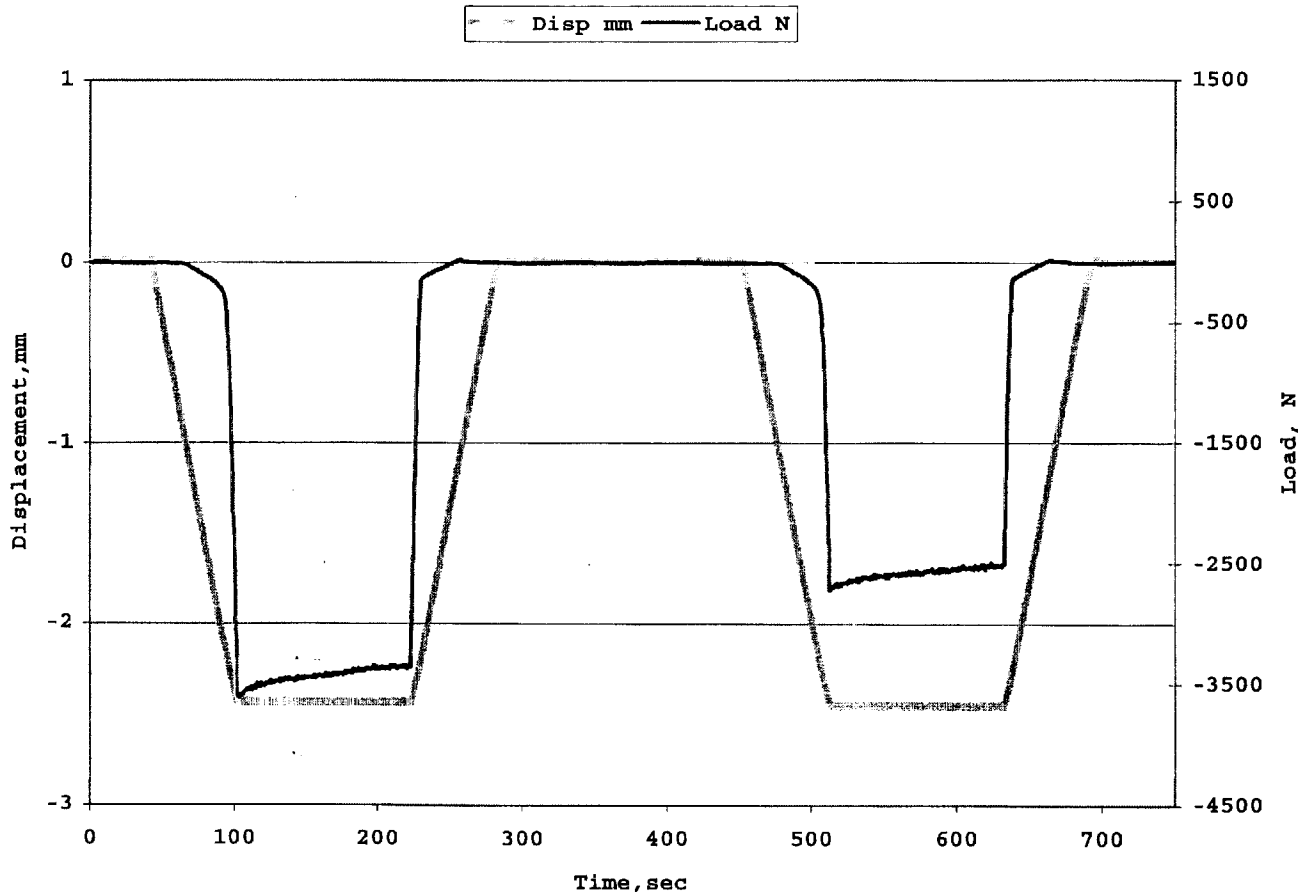

Figure 10: Axial Load and Displacement data plotted versus Test Time for the Volumetric Compression of SANTOPRENE Grade 101-73. Note two regions of recoverable stiffness, permanent set following first loading and relaxation of pressure after holding displacement.

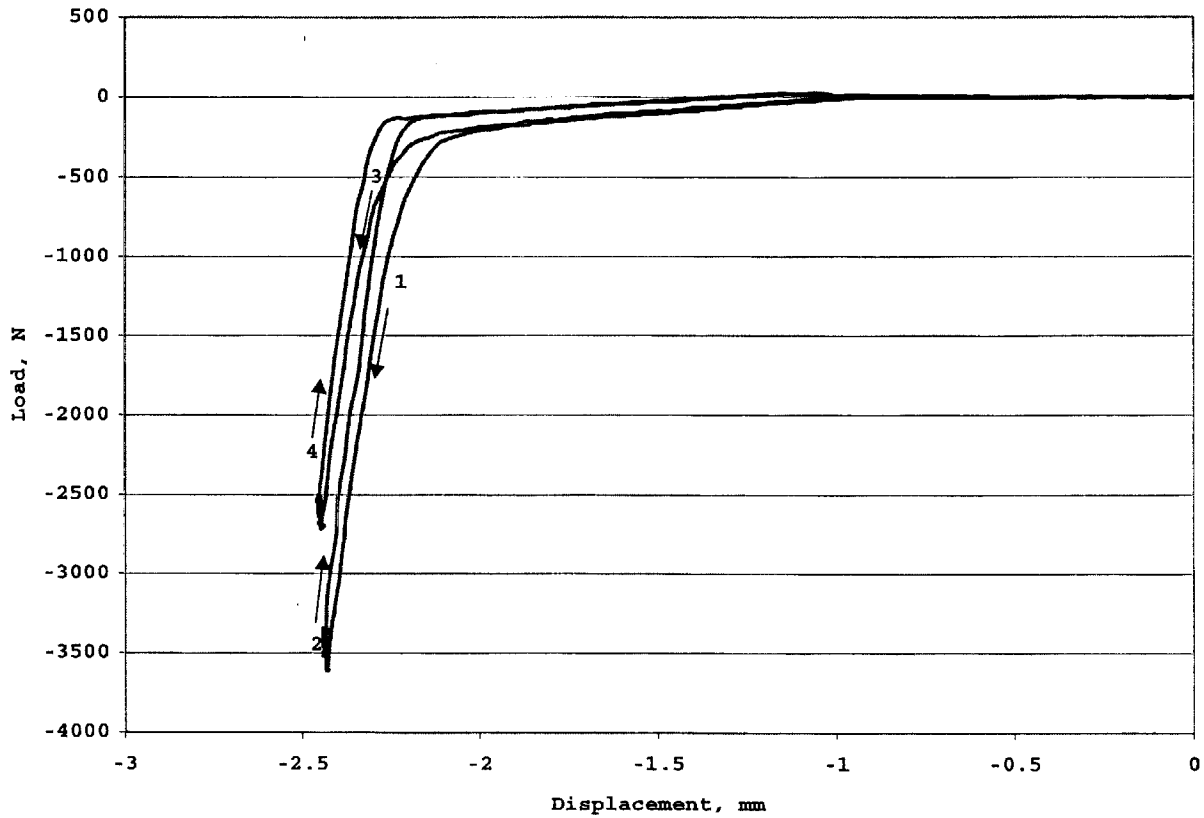

Figure 11: Load plotted versus Displacement for Volumetric Compression of SANTOPRENE Grade 101-73. Displacement sequence/direction is shown with numbers and arrows. The two recoverable bulk responses vary by nearly two orders of magnitude.

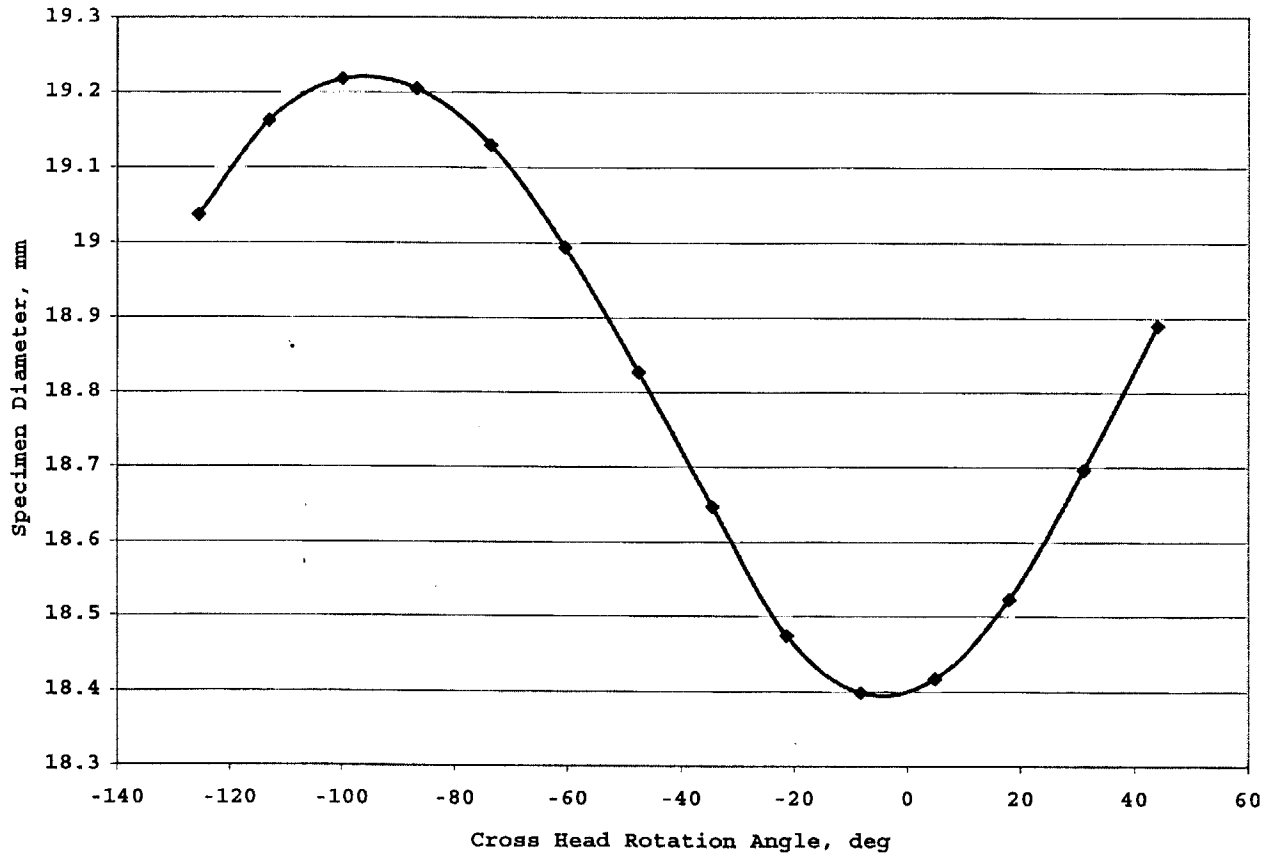

Figure 12: Diameter is plotted against rotation angle for an extruded SANTOPRENE rod specimen unclamped at its lower end, quantifying the non-circular cross-section of the specimen at a prescribed axial gage position.

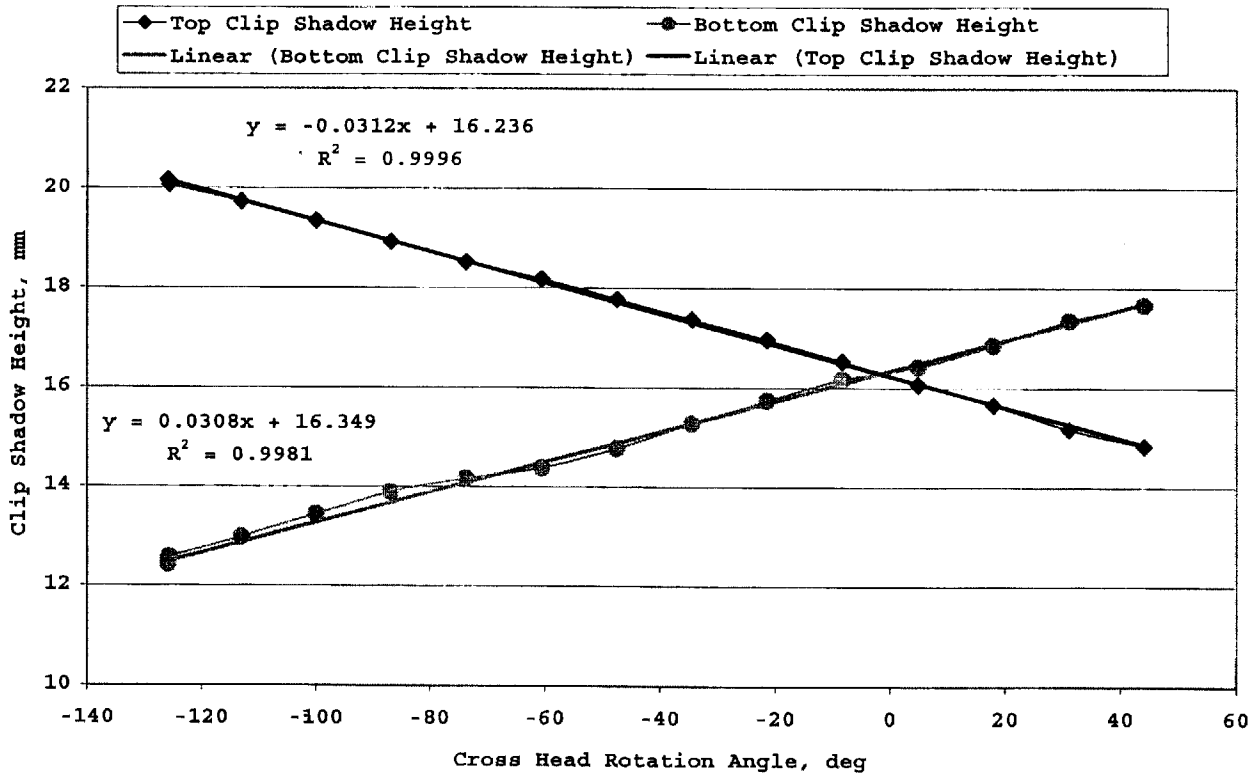

Figure 13: Rotation Calibration of Laser Gage Clips for tests with extruded rods of SANTOPRENE 101-73. Gage Clip Shadow Height is plotted against rotation angle for a specimen unclamped at its lower end.

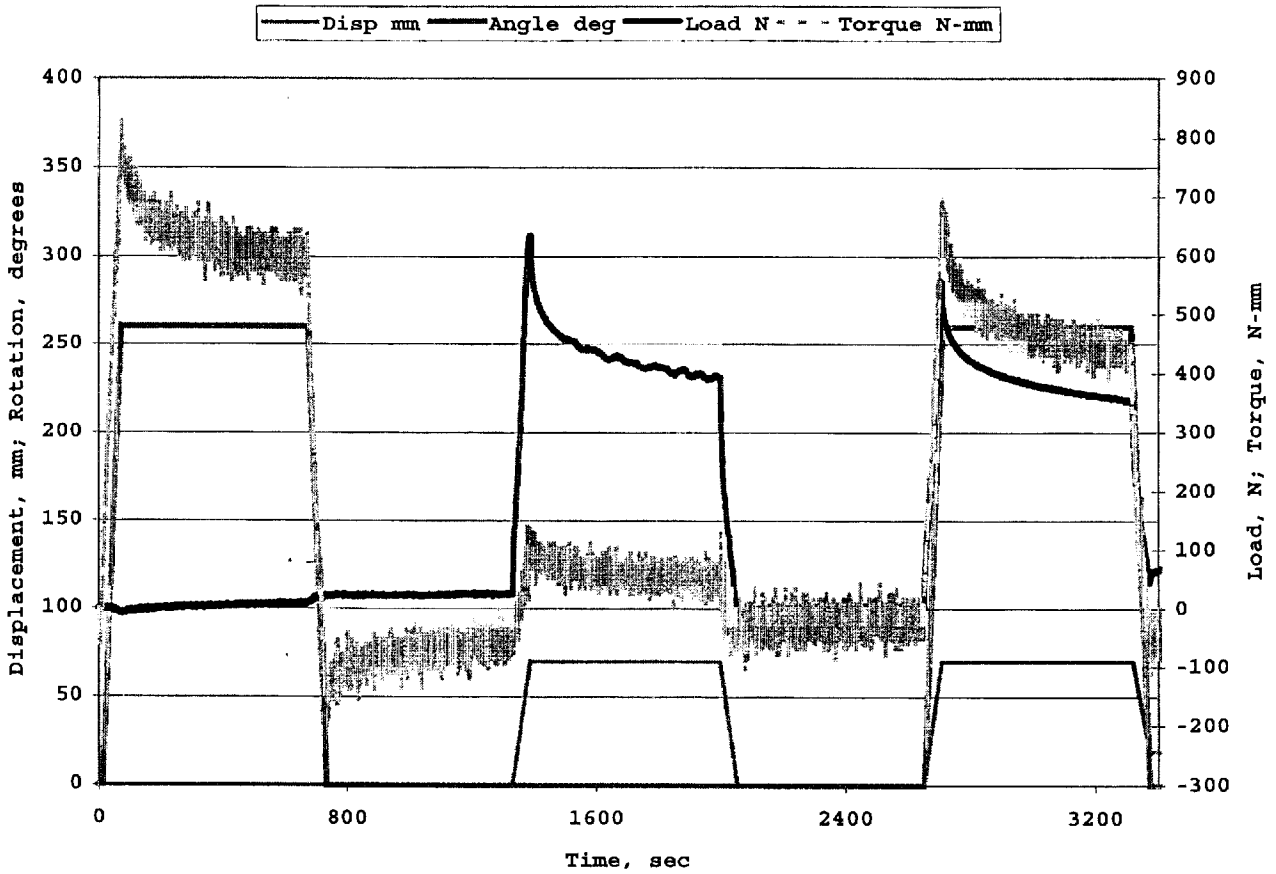

Figure 14: Raw displacement/load signal data for a SANTOPRENE Grade 101-73 sample undergoing a loading profile consisting of a simple torsional twist, a simple axial pull, then a concurrent torsional twist and axial pull.

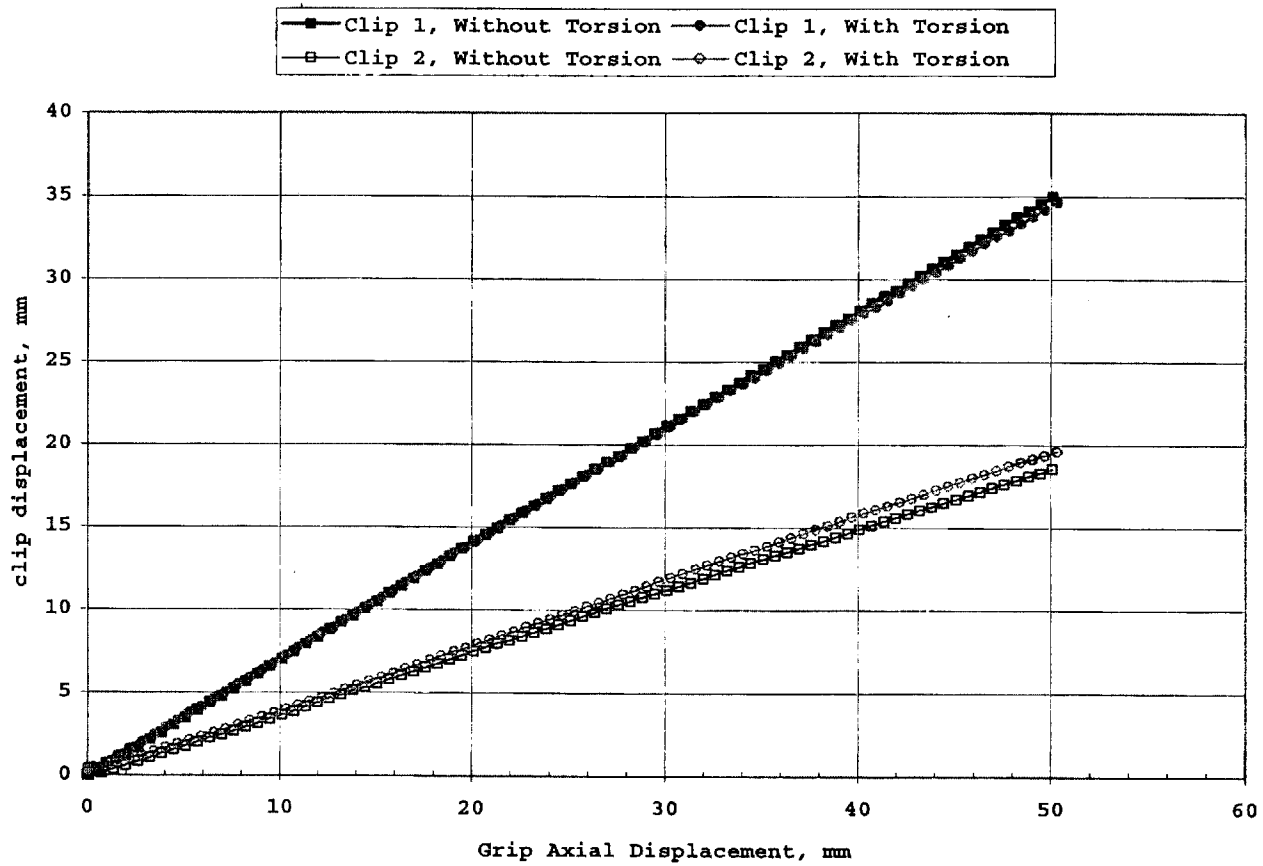

Figure 15: The effect of torsional twist on the relative axial displacements between laser clips during the axial deformations with and without a concurrent twist of a SANTOPRENE Grade 101-73 rod.

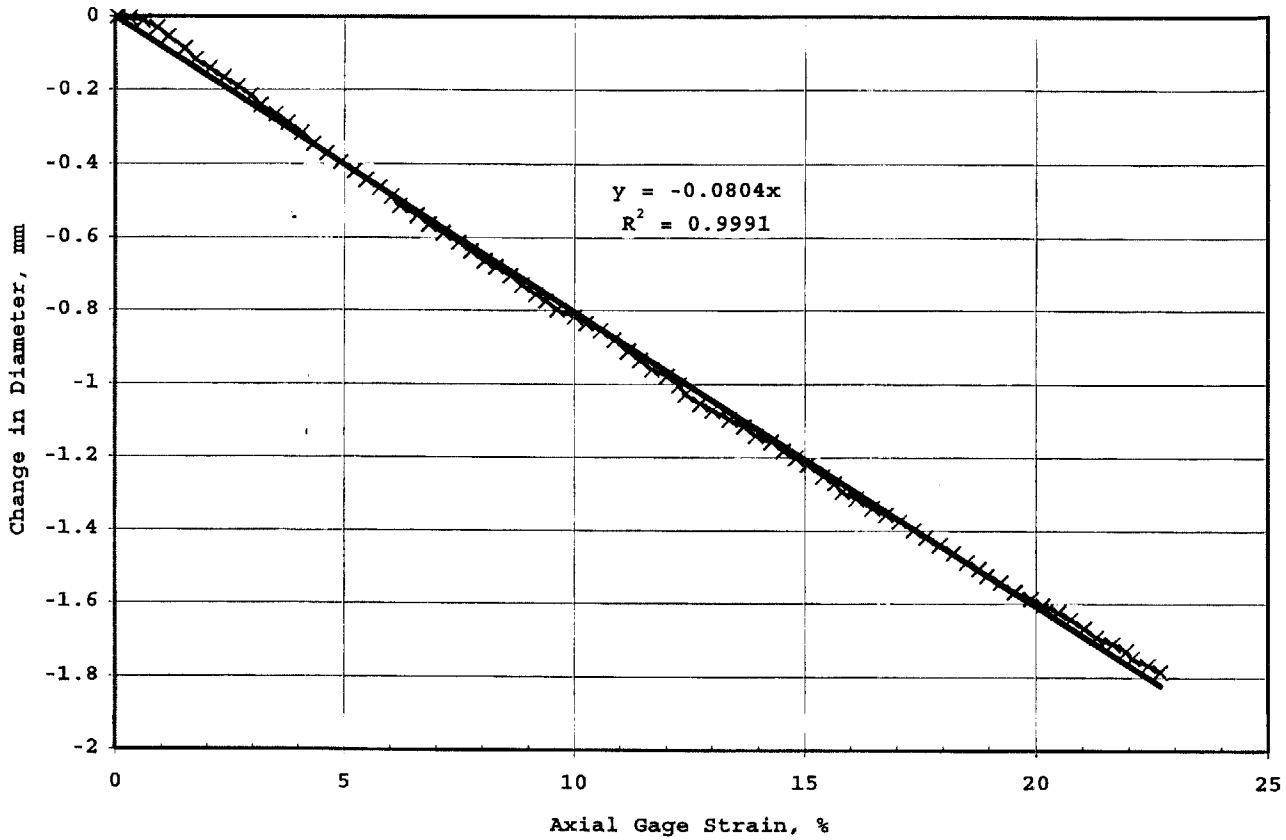

Figure 16: Change in sample diameter with axial gage strain measured during the simple axial pull of SANTOPRENE Grade 101-73 rod.

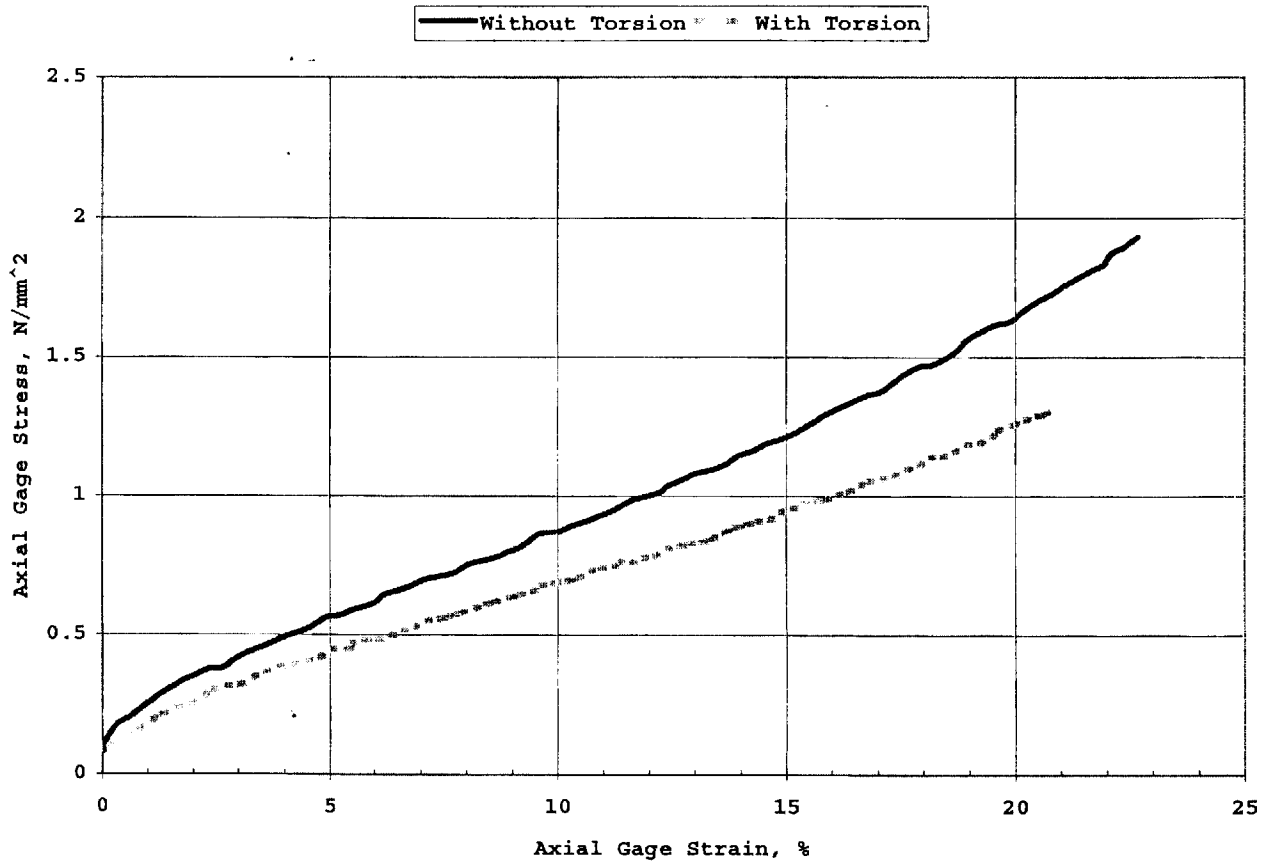

Figure 17: True Stress versus True Gage Strain curve plotted for the gage section of a SANTOPRENE Grade 101-73 rod, isolated by A/T laser clips. The concurrent twist effectively softens the axial response.

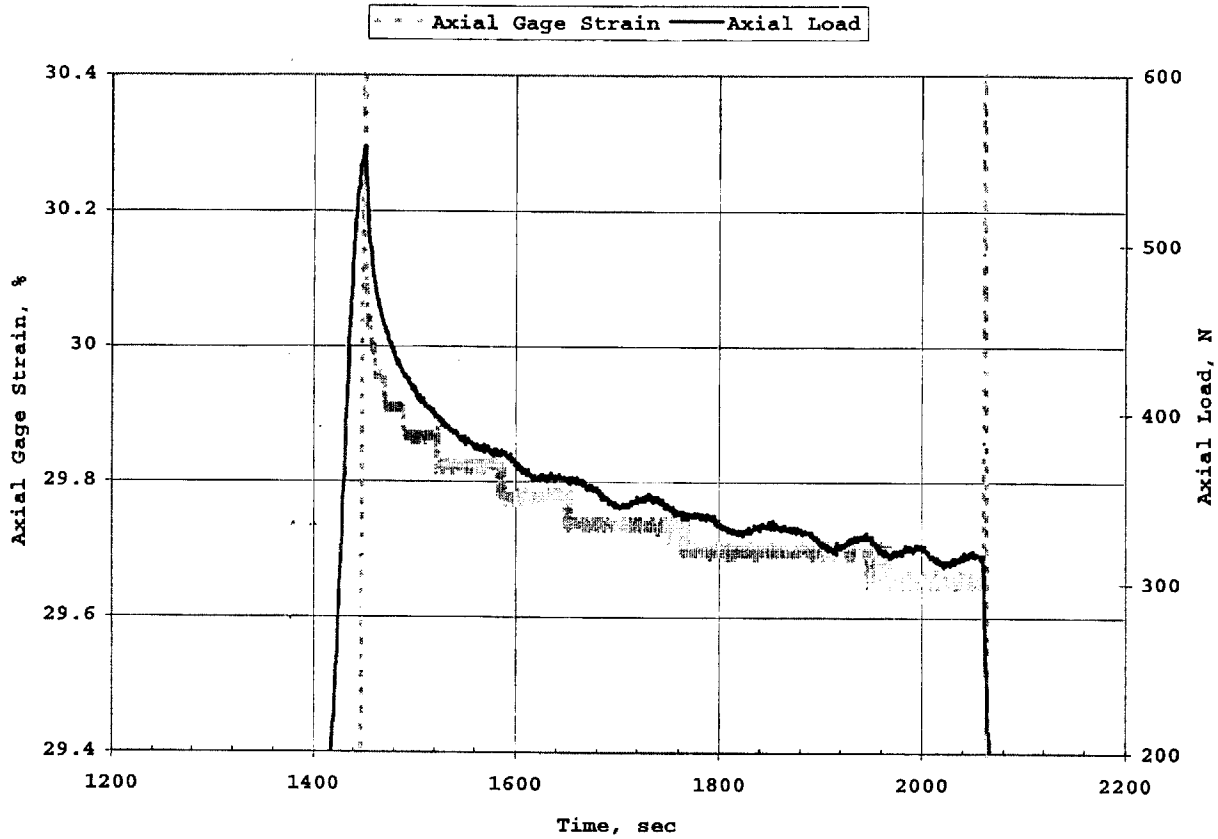

Figure 18: Relaxation of axial load and axial gage strain following isolated axial pull of a SANTOPRENE Grade 101-73 rod.

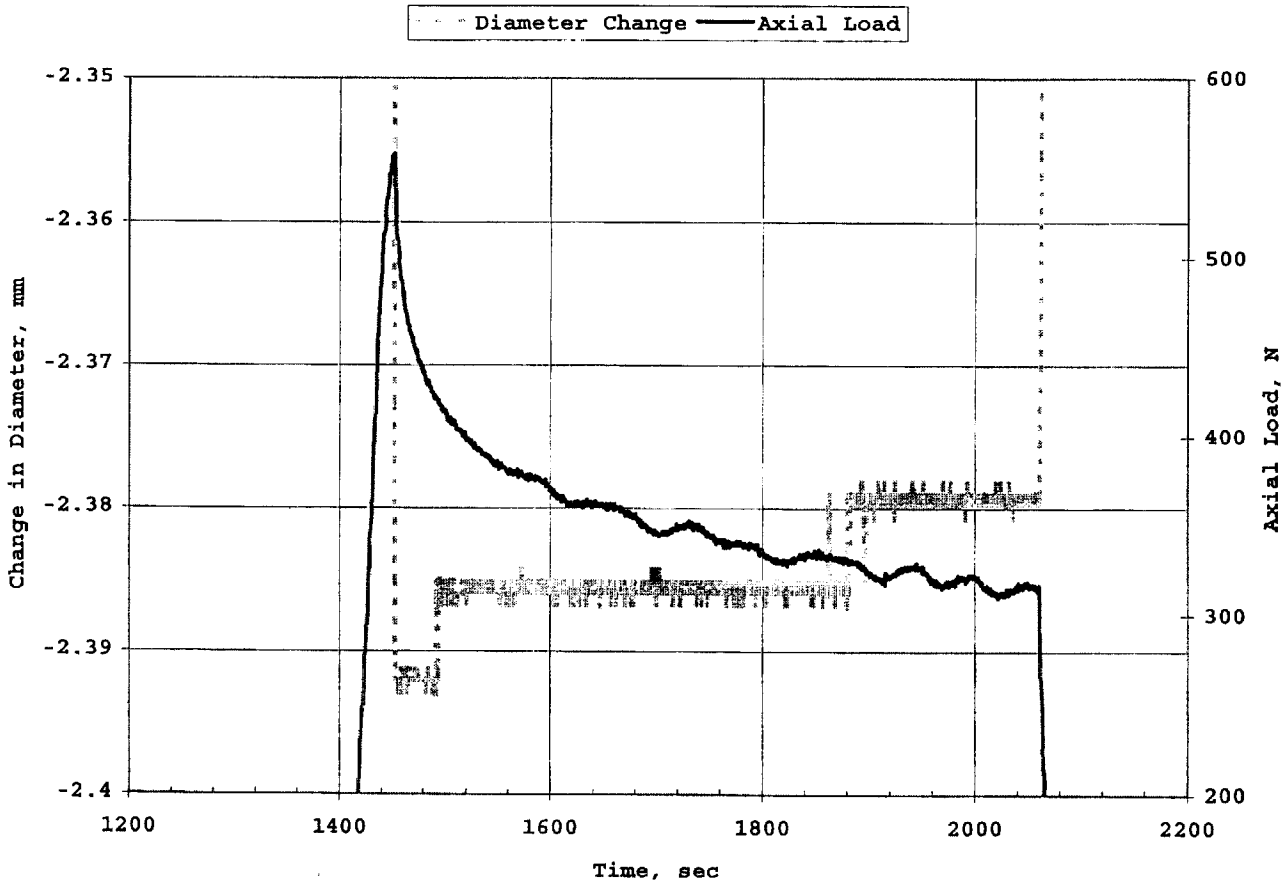

Figure 19: Relaxation of axial load and diameter change following isolated axial pull of a SANTOPRENE Grade 101-73 rod.

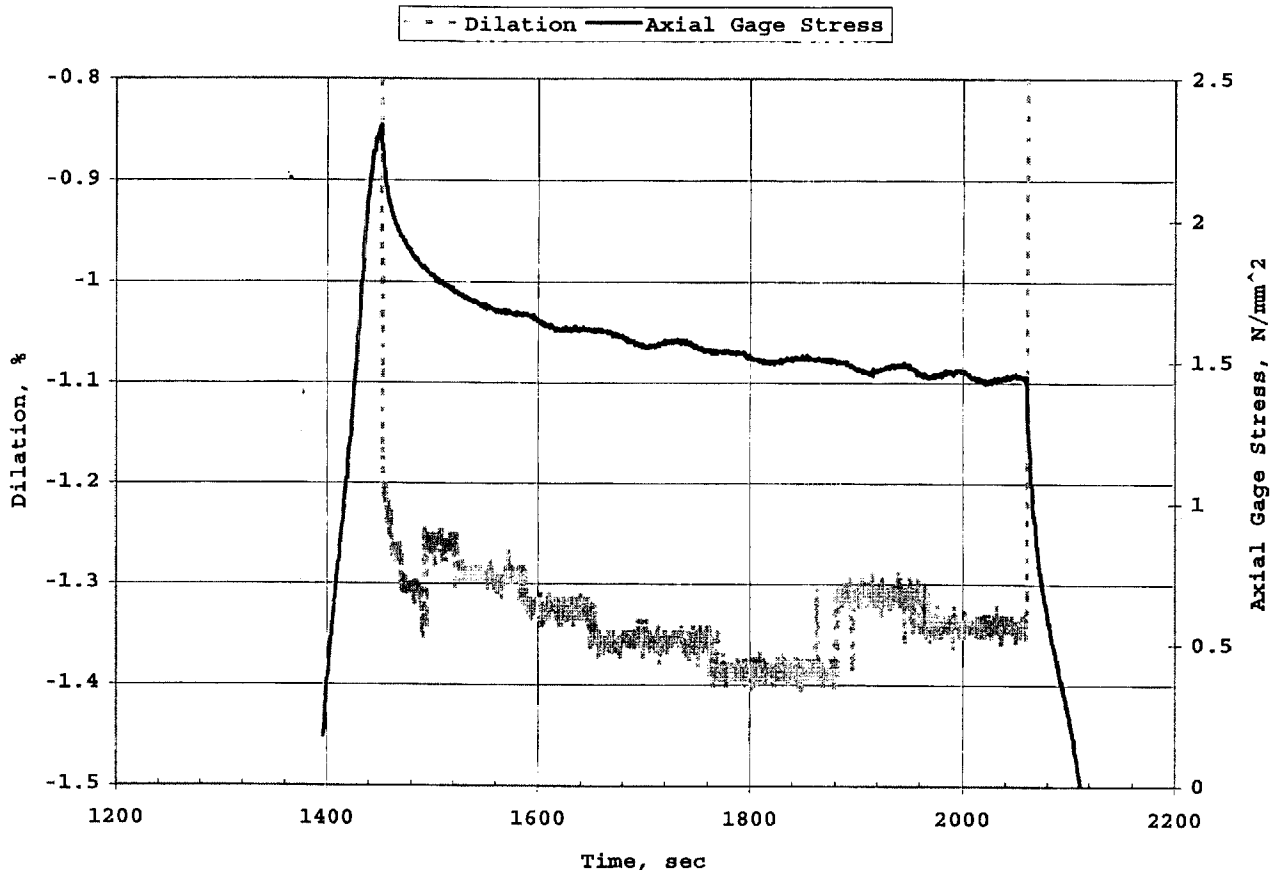

Figure 20: Relaxation of dilation and axial gage stress following isolated axial pull of a SANTOPRENE Grade 101-73 rod.

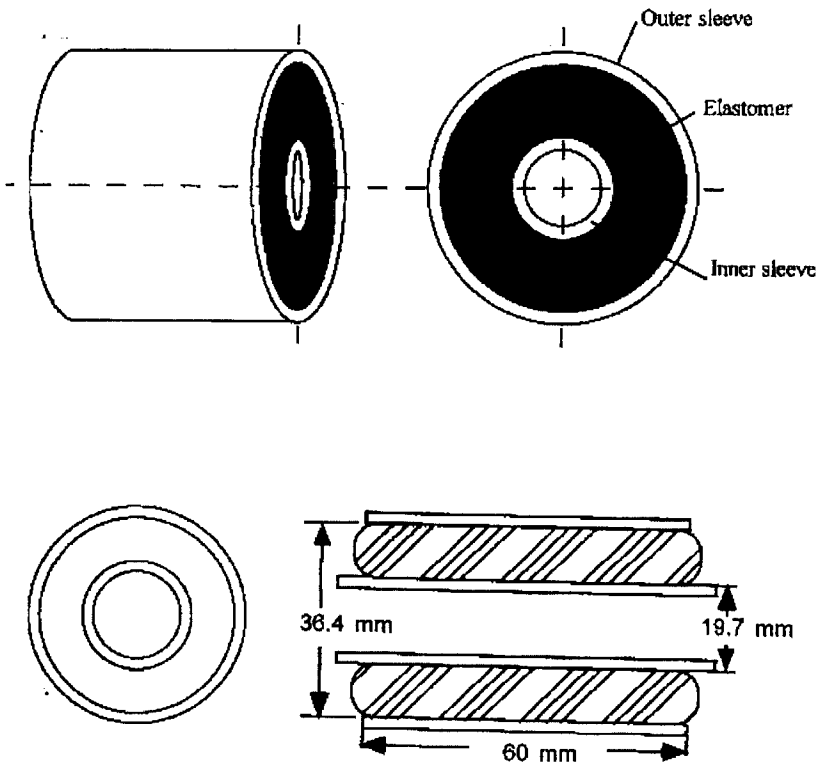

Figure 21: Bushing Test Specimen Geometry.

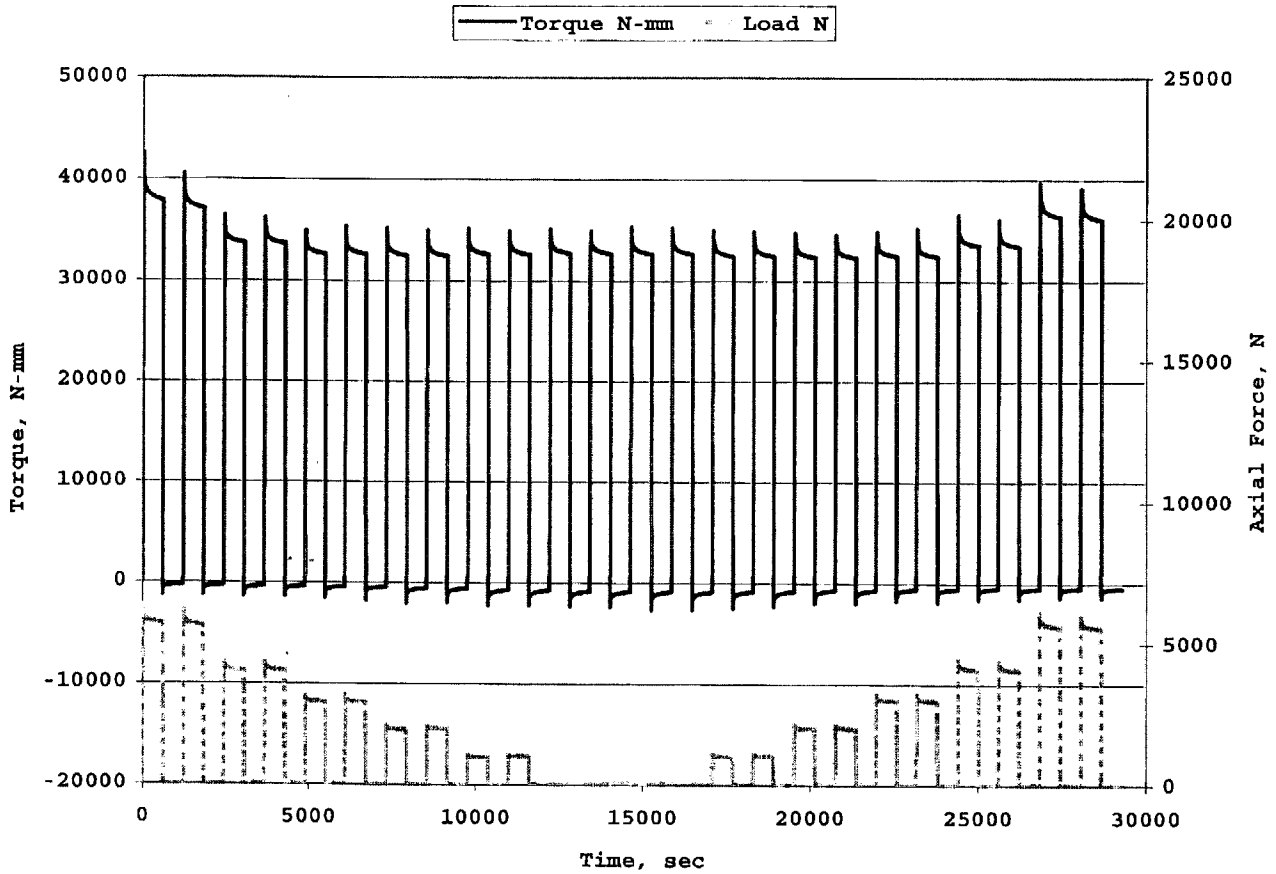

Figure 22: Load and torque output generated during a rubber bushing test in which the effect of changing displacement maximum effected the required torque for a rotation of 20 degrees.

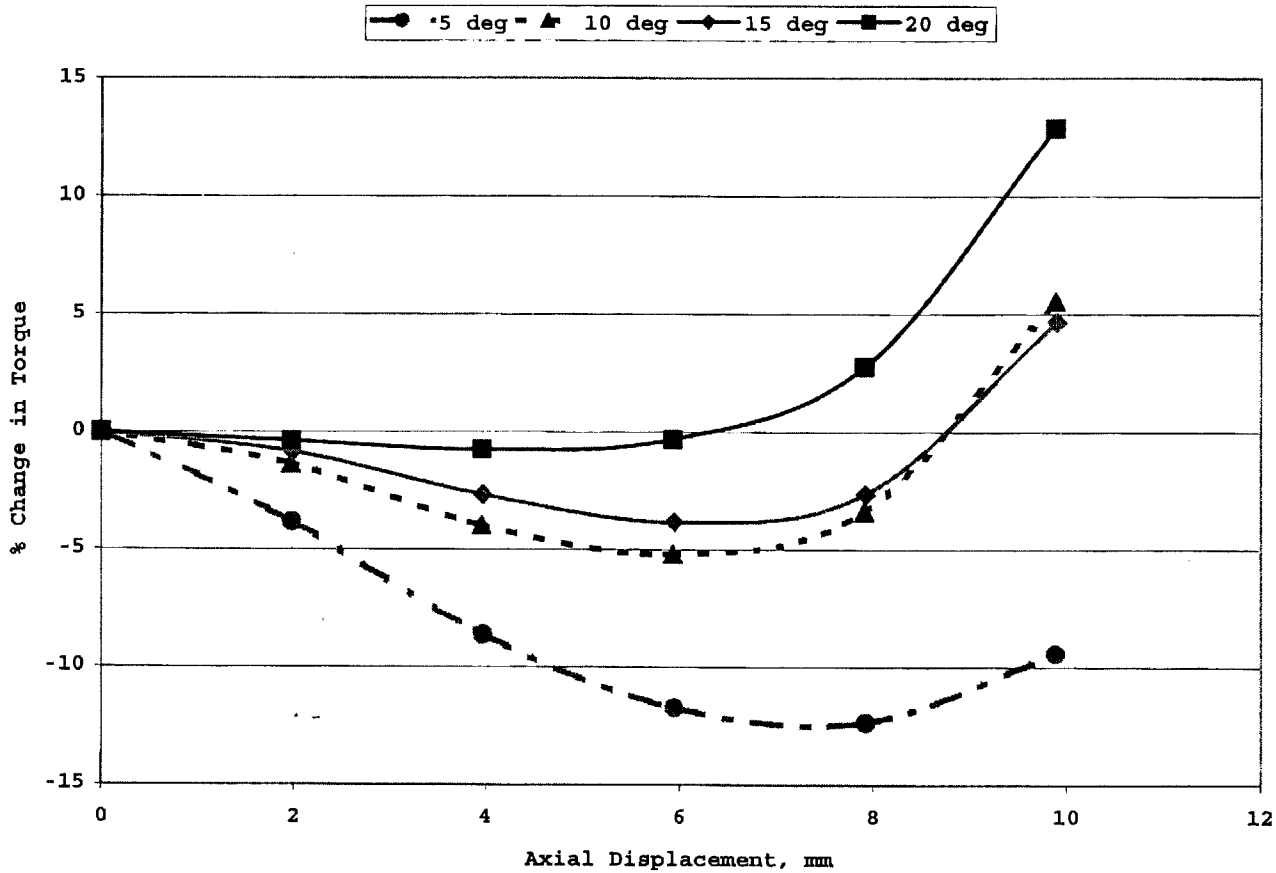

Figure 23: The effect of concurrent axial shear strain generated by axial displacement on the relative torsional response of a rubber bushing. The axial shear generates a softening and then hardening of the torsional stiffness as compared to the baseline generated with no concurrent axial displacement.

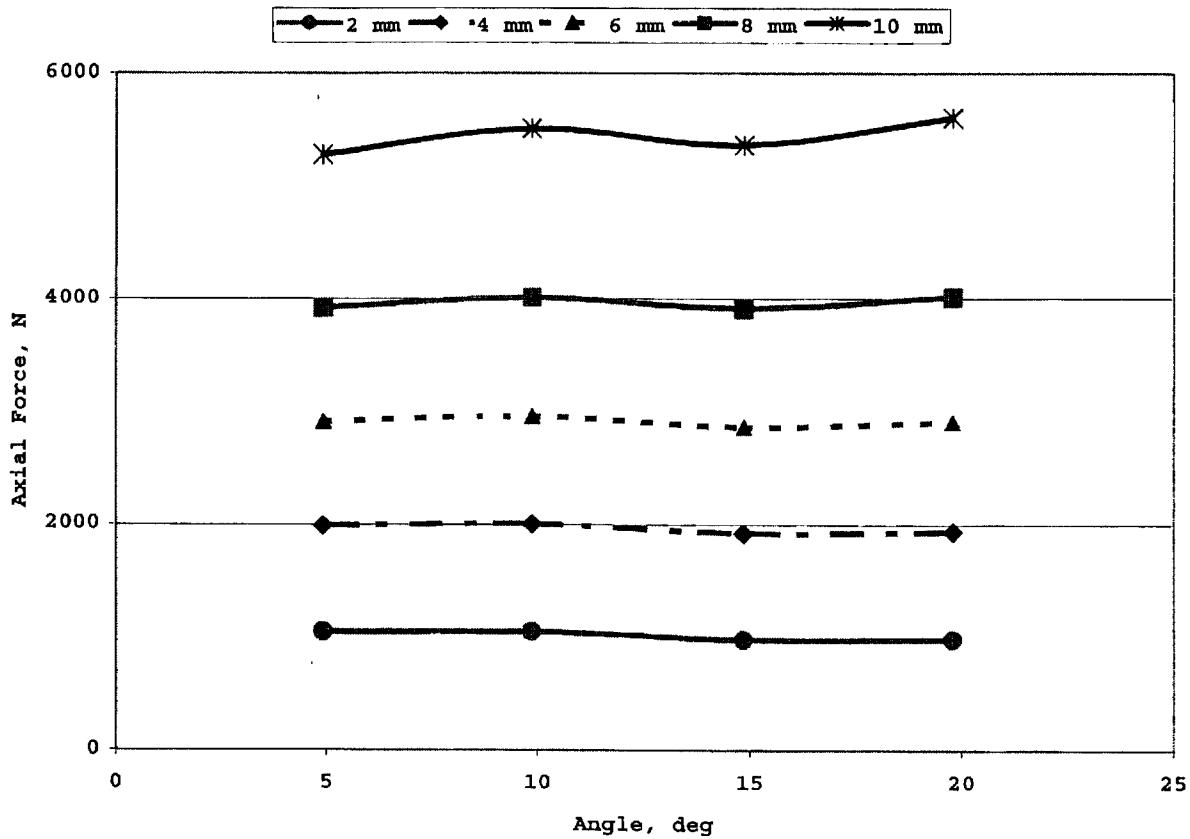

Figure 24: The effect of torsional shear generated by rotational twist on the absolute axial load response of a rubber bushing. The torsional shear produces no clear effect on the axial shear response.

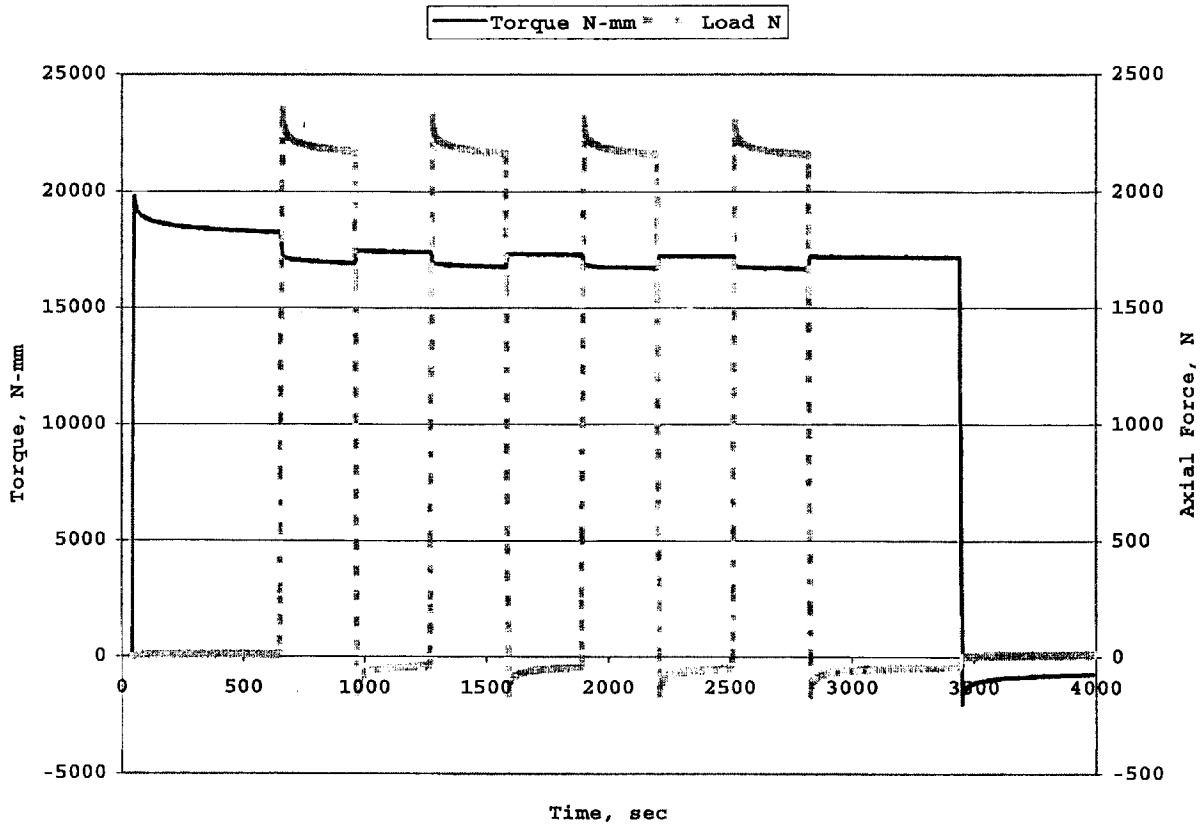

Figure 25: The effect of axial shear deformation on the relaxing torque required to hold fixed the rotational twist of a rubber bushing. The added deformation has an elastic and viscous effect on the response from the primary mode. The added axial shear appears to accelerate/augment the relaxation of the torsional stress.

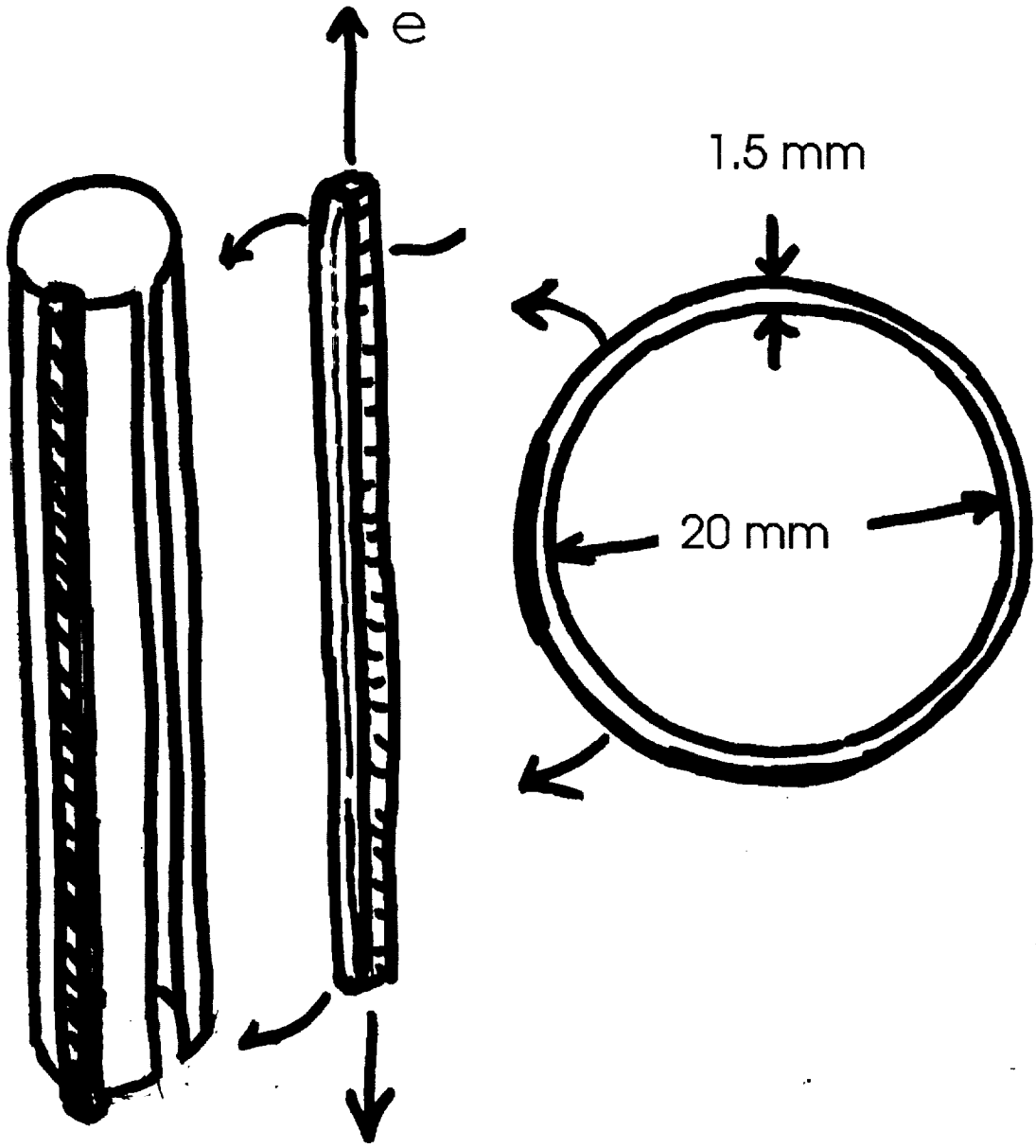

Figure 26: A schematic of the specimen and mounting used by Ornstein et al [3]. Stretched rubber band shaped specimens were stretched over copper plates of varying length that were bent along their width into the shape of cylinders

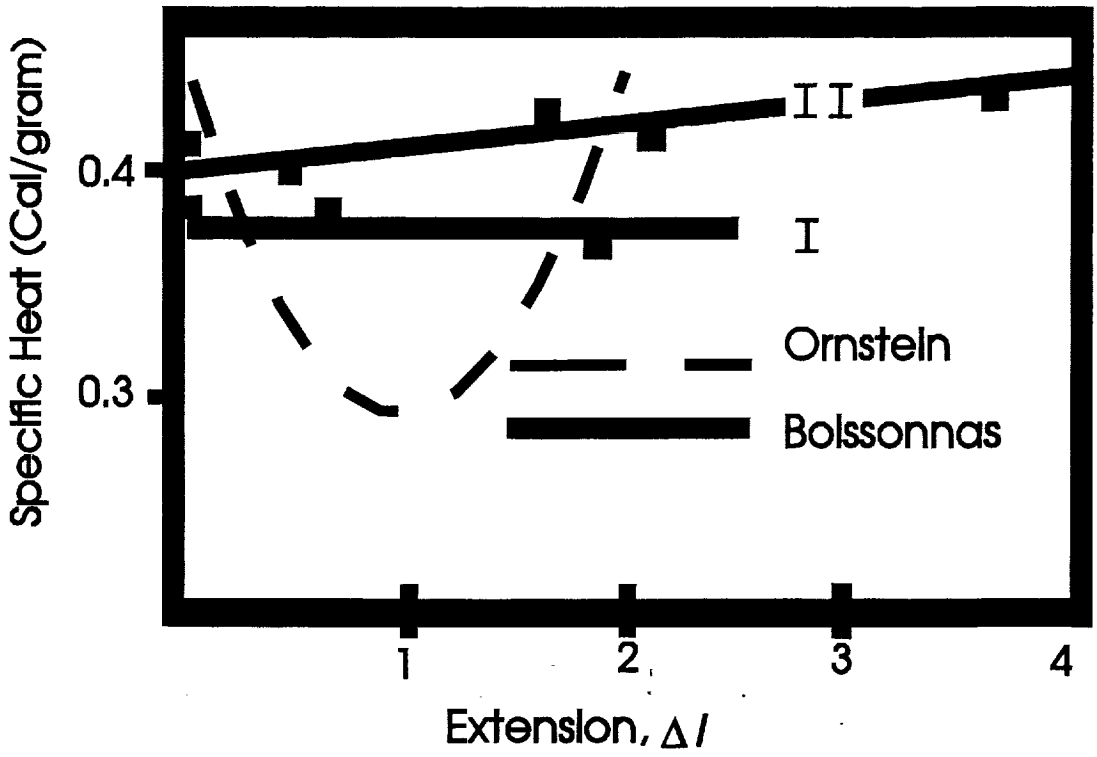

Figure 27: The results of Ornstein's experiments [3] suggest a strong and substantial dependence of heat capacity with strain. As strain was increased from 0 to 100% the rubber's average specific heat over the range of ~ 22-80° C fell by nearly a third and then increased back to the un-stretched value at a strain of 200%. The results of Boissonnas [4] are plotted as well.

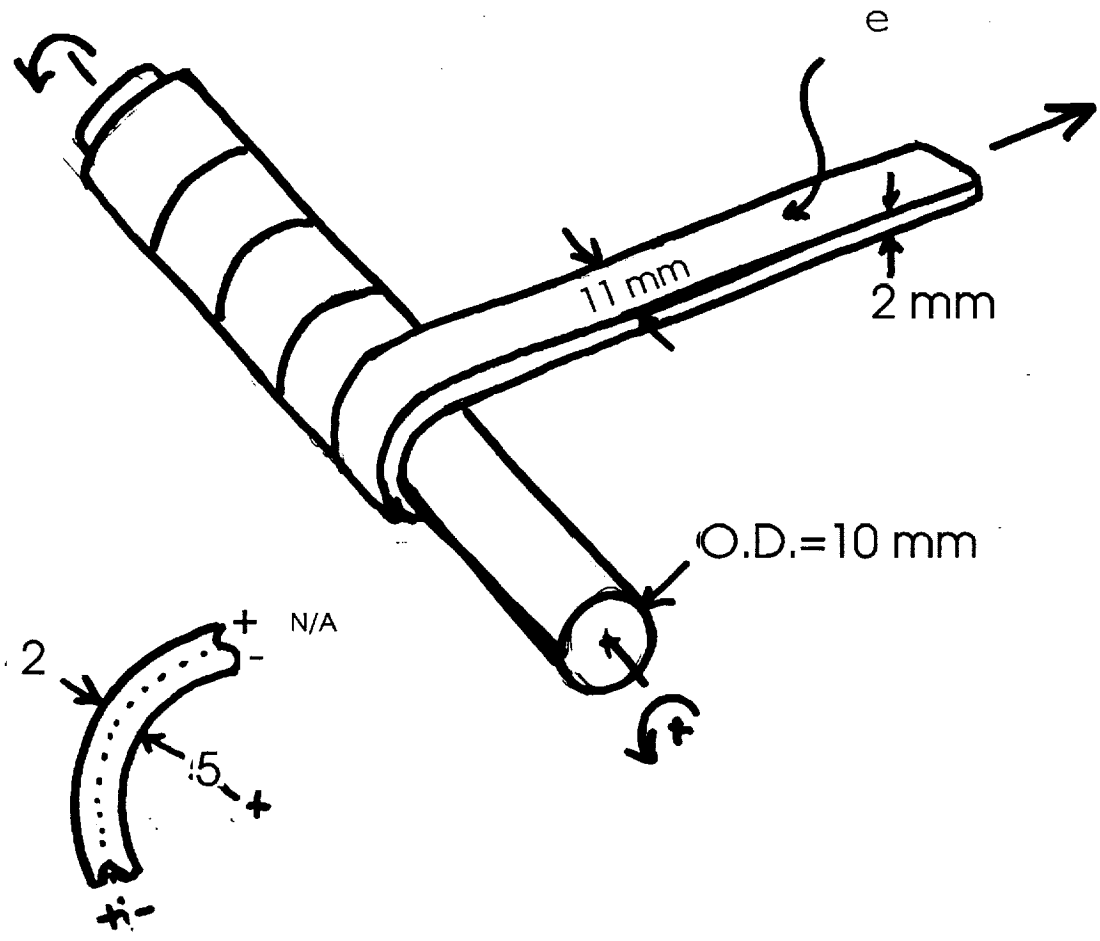

Figure 28: The specimen/mounting geometry of Boissonnas [4], rubber strips (1-2 mm thick) were cut from rubber sheets and stretched to given extensions with known weights. The strips were then wound over a cylindrical shaped electrical heating element.

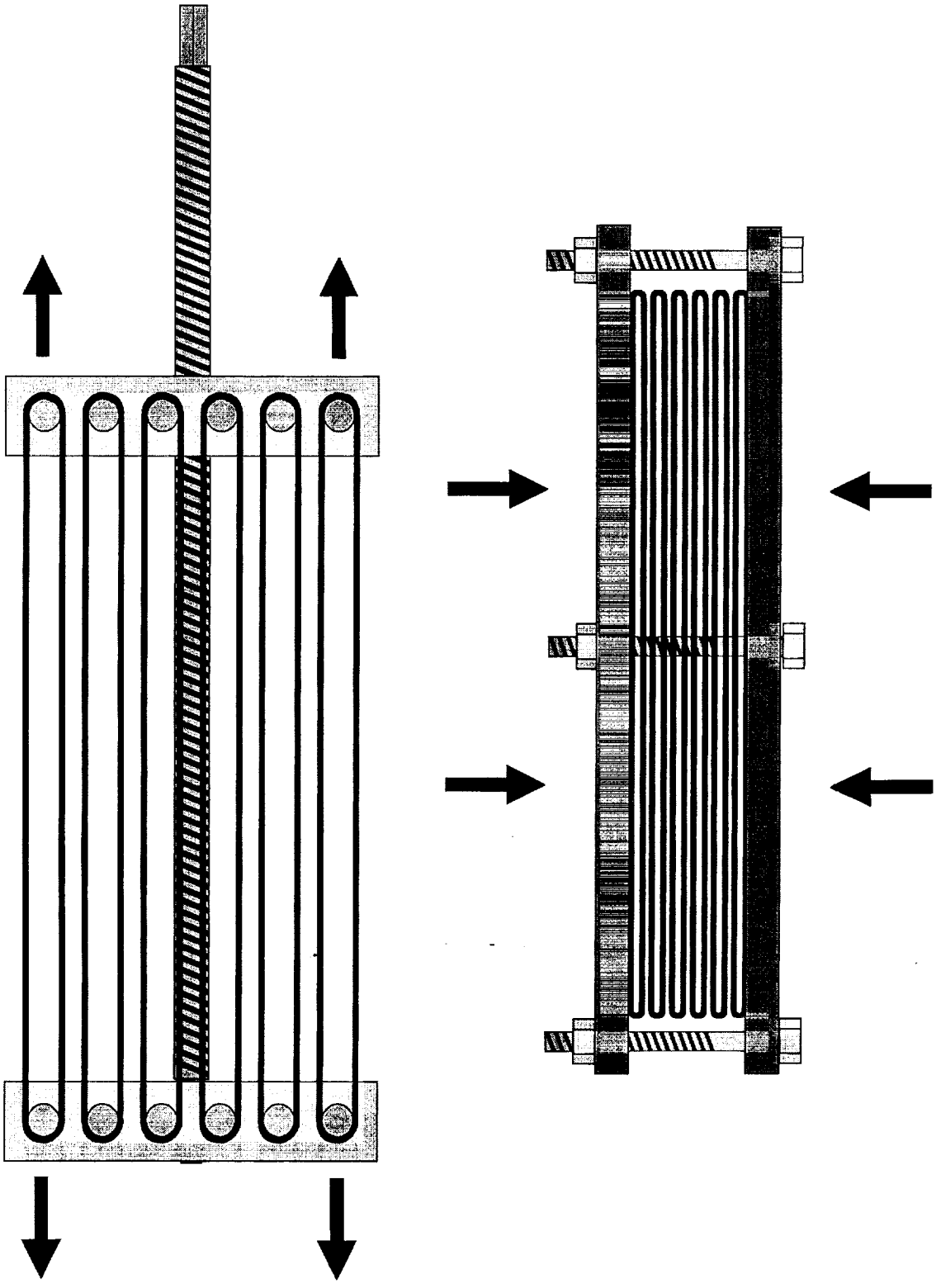

Figure 29: Schematic of test fixtures designed to examine effects of tension and compression strain on the heat capacity of rubber.